AGU PUBLICATIONS

Geochemistry, Geophysics, Geosystems

RESEARCH ARTICLE
10.1002/2014GC005672

Special Section:
Magnetism From Atomic to Planetary Scales: Physical Principles and Interdisciplinary Applications in Geo- and Planetary Sciences

Natural remanent magnetization acquisition in bioturbated sediment: General theory and implications for relative paleointensity reconstructions

R. Egli[1] and X. Zhao[2]

[1]Central Institute of Meteorology and Geodynamics (ZAMG), Vienna, Austria, [2]Department of Earth and Environmental Sciences, Ludwig-Maximilians University, Munich, Germany

Key Points:
- A natural magnetization is acquired in the mixed layer of bioturbated sediment
- The acquisition efficiency depends on the intensity of mixing
- Relative paleointensity artifacts depend on variable acquisition efficiencies

Supporting Information:
- Supporting Information S1

Correspondence to:
R. Egli,
ramon.egli@zamg.ac.at

Citation:
Egli, R., and X. Zhao (2015), Natural remanent magnetization acquisition in bioturbated sediment: General theory and implications for relative paleointensity reconstructions, *Geochem. Geophys. Geosyst.*, *16*, 995–1016, doi:10.1002/2014GC005672.

Received 1 DEC 2014
Accepted 6 MAR 2015
Accepted article online 16 MAR 2015
Published online 2 APR 2015

Abstract We present a general theory for the acquisition of natural remanent magnetizations (NRM) in sediment under the influence of (a) magnetic torques, (b) randomizing torques, and (c) torques resulting from interaction forces. Dynamic equilibrium between (a) and (b) in the water column and at the sediment-water interface generates a detrital remanent magnetization (DRM), while much stronger randomizing torques may be provided by bioturbation inside the mixed layer. These generate a so-called mixed remanent magnetization (MRM), which is stabilized by mechanical interaction forces. During the time required to cross the surface mixed layer, DRM is lost and MRM is acquired at a rate that depends on bioturbation intensity. Both processes are governed by a MRM lock-in function. The final NRM intensity is controlled mainly by a single parameter γ that is defined as the product of rotational diffusion and mixed-layer thickness, divided by sedimentation rate. This parameter defines three regimes: (1) slow mixing ($\gamma < 0.2$) leading to DRM preservation and insignificant MRM acquisition, (2) fast mixing ($\gamma > 10$) with MRM acquisition and full DRM randomization, and (3) intermediate mixing. Because the acquisition efficiency of DRM is larger than that of MRM, NRM intensity is particularly sensitive to γ in case of mixed regimes, generating variable NRM acquisition efficiencies. This model explains (1) lock-in delays that can be matched with empirical reconstructions from paleomagnetic records, (2) the existence of small lock-in depths that lead to DRM preservation, (3) specific NRM acquisition efficiencies of magnetofossil-rich sediments, and (4) some relative paleointensity artifacts.

1. Introduction

Understanding the acquisition of a natural remanent magnetization (NRM) by sediment settling in the Earth's magnetic field is a long-standing problem in paleomagnetism that has been subjected to detailed experimental and theoretical investigations for over 60 years [e.g., *Roberts et al*., 2013]. The two main NRM acquisition processes considered by these investigations are the depositional remanent magnetization (DRM), which is acquired during and shortly after deposition, and a delayed, so-called postdepositional remanent magnetization (PDRM). DRM acquisition models focus on flocculation of settling particles in the water column, particle rolling at the point of deposition [*Griffiths et al*., 1960; *Jezek et al*., 2012; *Bilardello et al*., 2013], and resuspension/reflocculation near the sediment-water interface [*Van Vreumingen*, 1993; *Katari and Tauxe*, 2000; *Tauxe et al*., 2006; *Heslop*, 2007; *Shcherbakov and Sycheva*, 2010]. On the other hand, PDRM is defined as a remanent magnetization that is acquired upon magnetic particle rotation against the yield strength of sediment until it is fully locked inside the consolidating layer [*Shcherbakov and Shcherbakova*, 1987; *Roberts et al*., 2013]. Delayed PDRM acquisition has been modeled by a so-called lock-in function, which represents the fraction of blocked PDRM as a function of depth below the surface mixed layer [*Bleil and von Dobeneck*, 1999; *Roberts and Winklhofer*, 2004; *Channell and Guyodo*, 2004; *Suganuma et al*., 2011].

The role of bioturbation as a possible PDRM acquisition mechanism was first considered by *Kent* [1973] and *Tucker* [1980], who assumed that remanence carriers could be realigned during sediment disturbance by benthic organisms. This type of PDRM originates inside the surface mixed layer, where benthic organisms are active, rather than below. Lock-in functions with nonzero contributions from the surface mixed layer have been proposed by *Channell and Guyodo* [2004]. Although the role of sediment mixing during PDRM

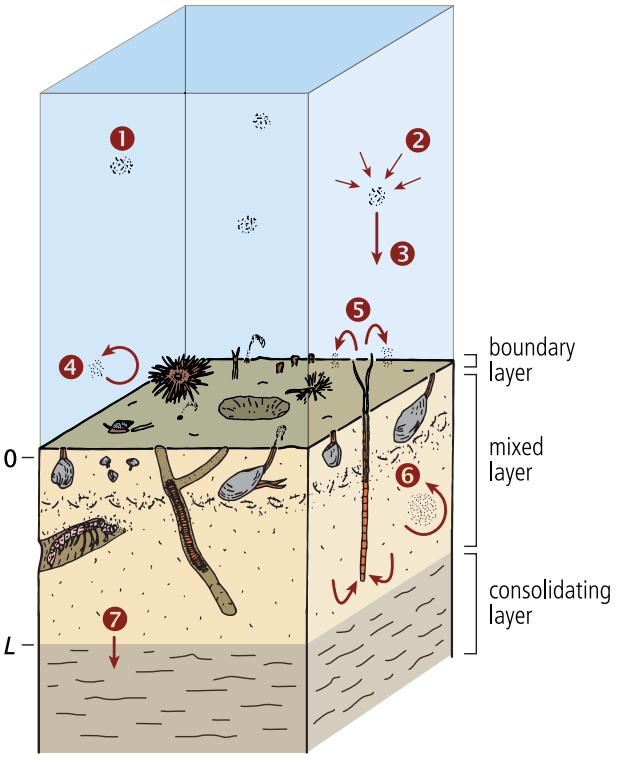

Figure 1. Schematic representation of processes that contribute to acquisition of sedimentary magnetizations. (1) Marine snow. (2) Flocculation (first step of DRM acquisition). (3) Settling. (4) Sediment resuspension (DRM renewal). (5) Nonlocal sediment mixing by polychaete worms. (6) Local (diffusive) sediment mixing (DRM randomization and MRM acquisition). (7) Transition to the consolidating layer (DRM and MRM locking).

acquisition has been recognized, the exact mechanism remains unclear. *Mao et al*. [2014a] explained laboratory PDRM acquisition in sediment containing living magnetotactic bacteria in terms of a dynamic equilibrium between aligning magnetic torques on the one hand, and randomizing forces due to sediment mixing on the other hand. With explicit reference to the physical alignment of magnetofossils, this type of PDRM has been referred to as "biogenic remanent magnetization" [*Heslop et al*., 2013], in order to distinguish it from the more general concept of biogeochemical remanent magnetizations acquired within a chemical lock-in zone [*Tarduno and Wilkison*, 1996; *Tarduno et al*., 1998; *Larrasoaña et al*., 2014]. Because bioturbation can affect a wide range of remanence carriers, including those with nonbiogenic origins, we use the term "mixing remanent magnetization" (MRM) for all types of remanent magnetizations acquired in sediment through internally driven mixing. As far as laboratory experiments are concerned, MRM is not necessarily identifiable with the PDRM acquired by sediment stirring [e.g., *Kent*, 1973], because, as we will discuss in section 2, bioturbation is characterized by specific mixing signatures.

The role of MRM as a source of NRM is unknown, given the existence of contradictory conclusions about DRM preservation inside the surface mixed layer. For example, *Katari et al*. [2000] reported substantial NRM preservation in marine sediments exposed to the burrowing activity of polychaete worms in a reversed polarity field for 3 weeks. On the other hand, simple calculations based on solid diffusion constants associated with bioturbation support the opposite conclusion that any original magnetic orientation will be randomized before magnetic particles reach the consolidating layer [*Mao et al*., 2014a]. The scope of the present paper is to provide a general model for remanent magnetization acquisition inside the surface mixed layer using a minimum set of physical parameters to characterize bioturbation and mechanical sediment properties. This model is used to explain important known aspects of NRM acquisition, namely (1) lock-in delays through a lock-in function that can be matched with empirical reconstructions based on paleomagnetic records, in particular those of *Channell and Guyodo* [2004], (2) the occurrence of DRM preservation and small lock-in depths for specific sedimentary settings [*Tauxe et al*., 2006], (3) the specific NRM acquisition efficiency of magnetofossil-rich sediments [e.g., *McNeill and Kirschvink*, 1993], and (4) variable NRM acquisition efficiency that can explain relative paleointensity artifacts [*Yamazaki et al*., 2013; *Ouyang et al*., 2014].

2. Sediment Mixing Models

Bioturbation is the phenomenon by which sediment is mixed by benthic organisms within the so-called benthic mixed layer, which generally comprises the topmost 2–20 cm of the sedimentary column (Figure 1). A consequence of this activity is that the age of the mixed layer is continuously reset, as seen from depth-invariant concentrations of age-dependent tracers (e.g., radionuclides) [*Boudreau*, 1994; *Trauth et al*., 1997]. While the influence of bioturbation on vertical sediment transport has been widely studied, possible effects

on the orientation of magnetic carriers are mostly unknown, so that opposite points of view exist on DRM preservation through the mixed layer, ranging from full preservation [e.g., *Katari et al*., 2000] to full destruction [e.g., *Mao et al*., 2014a]. Bioturbation models are usually divided into two main categories according to the invoked transport mechanism, i.e., local (diffusion-like) and nonlocal (advection-like). These two mechanisms affect the orientation of magnetic carriers in a specific manner, leading to different DRM preservation and MRM acquisition capabilities, as discussed in the following.

2.1. Nonlocal Mixing Models

The paradigm example of so-called nonlocal sediment mixing is represented by the activity of burrowing organisms, in particular polychaete worms (Figure 1). These worms transport sediment ingested at a certain depth by egesting it near the sediment surface [*Shull*, 2001]. This activity produces a conveyor belt-like vertical mixing of solid material: upward transport occurs inside the worms, while the surrounding sediment is slowly buried by the resuspended and redeposited material egested near the sediment surface. A new DRM is acquired during redeposition, so that the mixed layer is subjected to a continuous DRM renewal with no PDRM overprint [*Katari et al*., 2000]. Some other nonlocal sediment mixing mechanisms, such as crawling of crustaceans [e.g., *Solan et al*., 2004], are expected to work in a similar manner through sediment resuspension. On the other hand, burrowing activities unavoidably produce some small-scale (local) mixing: for example, polychaete worms release part of the ingested sediment in situ, without transporting it to the surface [*Shull*, 2001].

Nonlocal sediment transport is modeled through a so-called exchange function $K(z_1, z_2)$, which expresses the velocity of sediment transport from depth z_1 to depth z_2 [*Boudreau*, 1986b; *Meysman et al*., 2003] (see supporting information S0 for a list of symbols and mathematical notations used in this paper). Only exchange functions of the type $K(z_1, 0)$ can be expected to preserve magnetizations inside the mixed layer, because randomized sediment is supplied just at the sediment-water interface (i.e., $z_2=0$). However, more realistic models based, for instance, on exponential exchange functions of the type $K(z_1, z_2) \propto e^{-|z_1-z_2|/\lambda}$ [e.g., *Solan et al*., 2004] assume that sediment transport takes place between any pair of depths with consequent DRM loss. Nonlocal transport models cannot be solved uniquely with respect to tracer concentration profiles, so that arbitrary assumptions need to be made about the exchange function and the fraction of transported material subjected to DRM losses.

2.2. Local Mixing Models

Local mixing models represent sediment fluxes in terms of a solid diffusion process that depends on a single parameter: the self-diffusion or biodiffusion constant D_b, in units of length^2/time [*Boudreau*, 1986a; *Meysman et al*., 2003]. The random nature of solid diffusion at the level of individual sediment particles implies that any remanent magnetization becomes progressively overprinted. In most cases, radioactive tracer profiles can be fitted by assuming a depth-independent value of D_b over a layer of thickness L, which is identified with the surface mixed layer [*Reed et al*., 2006]. Local mixing models are widespread, because they provide simple estimates of the bioturbation depth L and the bioturbation intensity D_b. Values of D_b from 0.01 to 200 cm^2/yr in combination with mixing depths between 2 and 20 cm have been reported for various coastal, shelf, slope, and deep-sea sediments [e.g., *Boudreau*, 1994; *Teal et al*., 2008]. In reality, mixing depth estimates depend on tracer half-lives, as expected in the case of smoothly declining bioturbation rates at the bottom of the mixed layer. Some organisms are capable of burrowing to depths of 2 m [e.g., *Pemberton et al*., 1976]; however, such deep mixing is probably rare. D_b is proportional to sediment biomass, and thus to available nutrients [*Reed et al*., 2006]. A positive correlation with the organic carbon flux is also found for L, with an upper limit of $\sim$20 cm imposed by biological constraints [*Trauth et al*., 1997; *Boudreau*, 1998]. Finally, a weak positive correlation exists between D_b and the sedimentation rate ω, because nutrients are more abundant in coastal environments, where sediment accumulates more rapidly [*Boudreau*, 1994].

Diffusive material transport is described macroscopically by the translational Fick's law $\partial C/\partial t = D_b \Delta C$, where C is the concentration of a given substance. At the scale of individual sediment particles—defined here as elemental units that behave as individual elastic bodies—Fick's diffusion is equivalent to a random walk with net displacement $\langle r^2 \rangle = 6D_b t$ over time t [*Berg*, 1983]. By analogy, the orientation of individual particles subjected to random perturbations is equivalent to an angular random walk $\langle \theta^2 \rangle = 2D_r t$, where θ is the angle to an initial orientation, and D_r is the rotational diffusion coefficient in units of angle^2/time. The statistical

orientation of a large number of particles subjected to rotational diffusion is governed by the rotational counterpart of Fick's law, i.e.,

$$\frac{\partial p}{\partial t} = D_r \Delta p, \tag{1}$$

where $p = p(t, \theta, \varphi)$ is the probability density function of orientation vectors (e.g., magnetic moments) in spherical coordinates [*Perrin*, 1934, 1936]. While several studies exist on translational and rotational diffusion of colloidal suspensions, D_r has never been measured in sediment. Nevertheless, order-of-magnitude estimates of D_r can be obtained from translational diffusion. In the case of Brownian motion (i.e., particle movement caused by molecular collisions), rotational and translational diffusion are related by the Stokes-Einstein-Debye law

$$\frac{D_r}{D_b} = \frac{\Gamma_b}{\Gamma_r}, \tag{2}$$

where Γ_b and Γ_r are the translational and rotational viscous drag coefficients, respectively, which depend on particle shape and size. For the Brownian motion of spherical and disk-like particles of radius a [*Koenderink et al.*, 2003],

$$\left[\frac{D_r}{D_b}\right]_{\text{spheres}} = 2\left[\frac{D_r}{D_b}\right]_{\text{disks}} = \frac{3}{4a^2}. \tag{3}$$

The relation between translational and rotational diffusion of dense particle aggregates, such as sediments, is more complex and less well known. Significant deviations from the Stokes-Einstein-Debye relation have been reported for colloidal suspensions [*Koenderink et al.*, 2003] and colloidal clay gels [*Jabbari-Farouji et al.*, 2012], which means that translational and rotational diffusion can be decoupled by strong interparticle interactions. For example, the so-called cage effect, by which particles are confined inside void spaces, suppress particle translation but not rotation. Of particular interest for sediments is the case of colloidal clay gels, where D_r/D_b is lowered by up to 2 orders of magnitudes with respect to equation (3) [*Kim et al.*, 2011]. Bioturbation could have a similar effect through nonlocal transport mechanisms (section 2.1).

Generally, the orientation of isolated particles subjected to random perturbations in zero field is governed by equation (1) with a given initial distribution of magnetic moment directions. If the initial distribution is a function of the angle θ to a reference direction (i.e., an initially applied magnetic field) and the diffusion process is isotropic, the solution of equation (1) obtained from full initial alignment at $t = 0$ is given by

$$p(\theta, t) = \frac{1}{4\pi} \sum_{l=0}^{\infty} (2l+1)\, e^{-D_r l(l+1)\, t} P_l(\cos\theta), \tag{4}$$

where P_l are Legendre polynomials of order l (supporting information S1). The progressive magnetization loss during sediment mixing follows directly from equation (4) as [*Perrin*, 1934]

$$\frac{M}{M(t=0)} = \langle \cos\theta \rangle = e^{-2D_r t}. \tag{5}$$

This expression yields the half-life $t_{1/2} = \ln 2 / (2D_r)$ of any mixed-layer magnetization in zero field. The fraction of DRM surviving the transit of sediment through the mixed layer is obtained from equation (5) if t is identified with the mean residence time L/ω. In this case, we obtain $\langle \cos\theta \rangle = e^{-\gamma}$, where $\gamma = 2D_r L/\omega$ is what we shall call the (average) rotational diffusivity parameter of the surface mixed layer. We can now try to evaluate the fate of a DRM inside the mixed layer on the basis of D_r estimates obtained from equation (3). Using $a < 100\ \mu$m for the typical size of sediment particles [*Sverdrup et al.*, 1942] together with D_b estimates corresponding to various sedimentary settings listed in Table 1, we obtain $D_r > 150$ rad^2/yr and unrealistically small DRM half-lives of <20 h. On the other hand, luminophore imaging of ongoing macroscopic bioturbation are characterized by $a \approx 1$ mm [*Solan et al.*, 2004], in which case $D_r > 1.5$ rad^2/yr and $t_{1/2} < 84$ days. Even smaller diffusion values can be obtained on the basis of sub-Fickian rotational diffusion processes. In such cases, DRM might survive its journey through the mixed layer.

The problem with DRM survival estimates based on D_b is that an unknown fraction of the biodiffusion rate originates from the nonlocal transport processes discussed in section 2.1, whose efficiency in terms of

Table 1. Summary of Surface Mixed-Layer Properties for Selected Sedimentary Settings[a]

Location	ω (cm/kyr)	L (cm)	$D_{b,tr}$ (cm^2/yr)	$D_{b,bac}$(10 μm) (cm^2/yr)	D_r(10 μm) (rad^2/yr)	γ (10 μm)	DRM (%)
N Pacific gyre	0.2[b]	3.3 (2–6)[c]	0.02–0.3[d]	8×10^{-11}	6×10^{-5}	2	14–100
S Pacific gyre	0.2[b]	3.3 (2–6)[c]	0.02–0.3[d]	3×10^{-11}	2×10^{-5}	0.8	52–100
Eq. Pacific	0.5[b,c]	7 (5–8)[c]	0.2–0.3[d]	3×10^{-8}	0.02	600	0–94
Southern Ocean	0.31[e]	6 (5–7)[c]	0.1–0.7[d]	2.4×10^{-8}	0.02	700	0–93
NW Atlantic	5[f]	10 (9–12)[c]	0.65[g]	2.4×10^{-8}	0.02	70	0–99

[a]Explanations: ω is the sedimentation rate; L is the thickness of the mixed layer; $D_{b,tr}$ is the translational diffusion constant deduced from tracers; $D_{b,bac}$ is the estimated minimum translational diffusion constant associated with benthic microorganisms, based on $D_b = \varepsilon_{mob}(a_b/a)^2 N v D_B$ with $\varepsilon_{mob}=0.2$, $v \approx 0.03$ μm^3, $a_b=(3v/4\pi)^{1/3} \approx 0.2$ μm, $a=10$ μm, $D_B=0.1$ cm^2/yr, and N from *Kallmeyer et al.* [2012]. Values for $a=100$ μm are 100 times smaller. D_r is the minimum rotational diffusion constant deduced from $D_{b,bac}$ and equation (3) with $a=10$ μm. Values for $a=100$ μm are 10^4 times smaller. $\gamma=2D_rL/\omega$ is an estimate of the minimum rotational diffusivity parameter of the mixed layer, based on D_r and $a=10$ μm. The last column is the maximum relative fraction $e^{-\gamma}$ of DRM that survives bioturbation, based on $a=$10-100 μm.

[b]*Hammond et al.* [1996].

[c]*Pisias et al.* [1995].

[d]*Smith and Rabouille* [2002].

[e]*Geibert et al.* [2005].

[f]*Anderson et al.* [1988].

[g]Computed with equation (2) of *Boudreau* [1994].

rotational diffusion is unknown. In the following, we discuss a different strategy for obtaining a lower limit of D_r, which is based on bioturbation caused by microorganisms. Because the size of many microorganisms is comparable with that of sediment particles, the associated mixing action is of local nature by definition, greatly reducing uncertainties of D_r/D_b. On the other hand, direct measures of microscopic bioturbation rates are not available, except for some key observations related to magnetotactic bacteria living in sediment. Their poor (∼1%) alignment with the Earth's magnetic field contrasts with observations of the same bacteria in water, which demonstrates the existence of mechanical interactions between motile microorganisms and sediment particles [*Mao et al*., 2014a].

The displacement of motile microorganisms is governed by a biased random walk (chemotaxis) with self-diffusion coefficient D_B [*Berg*, 1983]. Collisions with nonmotile particles transmit part of this diffusion to the whole sediment, proportionally to the volume fraction ε of motile organisms [*Wilson et al*., 2011] and to the probability of mechanical interactions with sediment, which we assume to be proportional to the ratio between microorganism and sediment particle cross sections. Therefore, we set $D_b=\varepsilon(a_b/a)^2 D_B$ for microorganism-driven solid diffusion in sediment, where a_b and a are the radii of microorganisms and sediment particles, respectively. Furthermore, $\varepsilon=\varepsilon_{mob}Nv$ is deduced from benthic microbial abundances N in cells/cm^3 [*Kallmeyer et al*., 2012], mean cell volumes $v \approx 0.03$ μm^3 [e.g., *Cole et al*., 1993; *Šestanović et al*., 2005], and fraction $\varepsilon_{mob} > 0.2$ of motile microbes [*Fenchel*, 2001; *Mitchell and Kogure*, 2006]. Finally, microscopy of cultured bacteria suspensions yields $D_B \approx 0.1$ cm^2/yr [*Wilson et al*., 2011; *Martinez et al*., 2012], while $D_B \approx 1$ cm^2/yr can be deduced from the displacement of magnetotactic bacteria in sediment shielded from magnetic fields (i.e., $\langle r^2 \rangle = 0.2$ cm over 14 days, *Mao et al*. [2014b]).

Using the most conservative estimates of D_B in combination with $a \approx$ 10-100 μm and $a_b \approx 0.2$ μm, we obtain D_r values comprised between 6×10^{-9} and 0.02 rad^2/yr (Table 1), which, being based only on part of the whole benthic community, should be considered as a lower limit of rotational biodiffusion. Accordingly, upper limits for the DRM fraction that survives bioturbation are comprised between ∼0 and ∼100%, depending on the sedimentary setting (Table 1). The best chances of DRM survival occur in nutrient-poor (i.e., small D_rL) and rapidly accumulating sediment (i.e., large ω), where $\gamma < 1$. Even if our estimates are affected by order-of-magnitude uncertainties, they provide strong evidence for the possibility that significant fractions of the total NRM can be acquired inside the surface mixed layer. Furthermore, cases with partial DRM preservation listed in Table 1 are of particular interest for relative paleointensity reconstructions, because, as we will see later, different DRM and PDRM acquisition efficiencies can lead to NRM fluctuations driven by the rotational diffusivity γ of the surface mixed layer.

3. Equilibrium Solutions for Particle Orientations in Water and Sediment

The orientation of sediment particles is controlled by the simultaneous action of (a) driving forces (i.e., bioturbation and Brownian motion), (b) viscous forces, (c) many-body interaction forces (e.g., hard contacts,

electrostatic, and Van der Waals), and (d) external forces (gravity and magnetic torques). The nature of most forces is extremely complex and unknown in detail; therefore, we approach the problem in a statistical manner. Torques are conveniently defined as the gradient $-\nabla V$ of a so-called torque potential $V(\theta,\varphi)$ expressed in spherical coordinates (θ,φ), where θ is the angle to the applied field. In this case, magnetic torques are generated by $V=-mB\cos\theta$, where B is the ambient field and m the magnetic moment of individual sediment particles or flocs. On the other hand, the random nature of interactions with neighbor particles is best described by an appropriately defined random potential, as shown later in section 3.2.

The probability density function $p=p(t,\theta,\varphi)$ of particle orientations subjected to rotational diffusion in a torque potential V is governed by the so-called Smoluchowski-Debye equation

$$\frac{\partial p}{\partial t}=D_r\Delta p+\frac{1}{\Gamma_r}\nabla(p\,\nabla V), \tag{6}$$

where Γ_r is the rotational viscous drag coefficient. This coefficient depends on the size and shape of the diffusing particles: for example, $\Gamma_r=8\pi\eta a^3$ for spheres with radius a immersed in a fluid with dynamic viscosity η. Under stationary conditions, p reaches a dynamic equilibrium with the ambient field, fulfilling equation (6) with $\partial p/\partial t=0$. The general solution of the Smoluchowski-Debye equation at equilibrium is the Boltzmann distribution

$$p(\theta,\varphi)=p_0\exp\left(\frac{-V(\theta,\varphi)}{D_r\Gamma_r}\right), \tag{7}$$

where p_0 is a constant ensuring that the total probability associated with p is 1 (supporting information S2). The expected magnetization M resulting from magnetic moment orientations with distribution p is obtained by integrating the z-components of the moment vectors over the unit sphere, i.e.,

$$\frac{M}{M_0}=\int_{\varphi=0}^{2\pi}\int_{\theta=0}^{\pi}p(\theta,\varphi)\cos\theta\sin\theta\,\mathrm{d}\theta\,\mathrm{d}\varphi, \tag{8}$$

where M_0 is the maximum magnetization obtained from full alignment in the external field.

In the following, we discuss specific solutions of the Smoluchowski-Debye equation representing limit cases of particles or flocs with negligible interactions, as typically encountered in the water column and near the sediment-water interface, and with strong interacting forces, as expected in the mixed layer, and more so in the consolidating layer.

3.1. Isolated Particles in a Perturbed Medium

We assume magnetic particles to be suspended in a viscous medium, with rotational diffusion originating from Brownian motion or from turbulence. The sole potential acting on the particles originates from magnetic torques, i.e., $V=-mB\cos\theta$. In this case, equation (7) yields the well-known Fisher-Von Mises distribution [*Fisher*, 1953]:

$$p(\theta)=\frac{\kappa}{4\pi\sinh\kappa}e^{\kappa\cos\theta}, \tag{9}$$

with $\kappa=mB/(D_r\Gamma_r)$. The associated magnetization obeys a Langevin law with

$$\frac{M_{eq}}{M_0}=\boldsymbol{L}\left(\frac{mB}{D_r\Gamma_r}\right), \tag{10}$$

where $\boldsymbol{L}(x)=\coth x-1/x$ is the Langevin function. The fluctuation-dissipation theorem gives $D_r=k_BT/\Gamma_r$ for the case of Brownian motion, where k_B is the Boltzmann constant and T the absolute temperature, so that

$$\frac{M_{eq}}{M_0}=\boldsymbol{L}\left(\frac{mB}{k_BT}\right) \tag{11}$$

describes the alignment of magnetic particles in undisturbed fluids. This solution has been used to quantify the statistical alignment of magnetic bacteria in water [*Frankel and Blakemore*, 1980; *Mao et al.*, 2014a, 2014b]. An important generalization of equation (11) is obtained if k_BT, which is the mean torque of

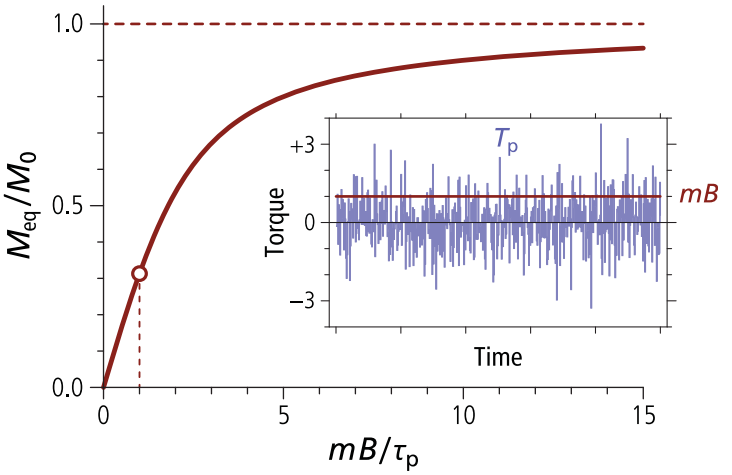

Figure 2. Normalized equilibrium magnetization, M_{eq}/M_0, of particles with magnetic moment m in a magnetic field B, when subjected to random perturbing torques T_p with zero mean and standard deviation τ_p. The magnetization corresponding to $mB/\tau_p=1$ is marked by a dot, with a sequence of 500 perturbations shown in the inset.

perturbations arising from molecular collisions, is replaced by the mean torque τ_p of unspecified random perturbations (Figure 2), i.e.,

$$\frac{M_{eq}}{M_0}=\boldsymbol{L}\left(\frac{mB}{\tau_p}\right). \qquad (12)$$

An essential condition for the validity of equation (12) is that flocs behave as discrete bodies with negligible reciprocal interaction forces. For example, τ_p can be identified with the amplitude of hydrodynamic torques from small vortices created by magnetic flocs sinking in the water column [*Heslop*, 2007]. In this case, equation (12), along with an appropriate description of flocculation dynamics [*Shcherbakov and Sycheva*, 2010], governs DRM acquisition. Using the calculations of *Heslop* [2007], equation (12) yields $M_{eq}/M_0=0.88$ for 8 μm flocs with an aspect ratio of 1.1 sinking in a 50 μT field, and $M_{eq}/M_0=0.09$ for 12 μm flocs. This example illustrates the well-known problem of nonlinear DRM acquisition by smaller flocs [*Tauxe et al*., 2006].

3.2. Equilibrium Magnetization in Mixed Sediment

Mao et al. [2014a] used equation (12) to explain PDRM acquisition experiments in sediments with 68–88% porosity, identifying τ_p with the typical energy of microscopic bioturbation events. A serious limit of this approach is represented by the fact that individual sediment particles (defined as the smallest units with elastic body behavior) are not independent from each other, as required by equation (12). Instead, a dense network of interparticle forces grows rapidly below the sediment-water interface, as seen in colloidal suspensions upon reaching a critical packing fraction [*Weitz*, 2011]. This network holds individual particles in place against random perturbations and is responsible for the rheological response of sediment to mechanical stresses. As with the case of random perturbations, we are interested in particle rotation and represent holding forces in terms of torques derived from a so-called "holding" potential $U(\theta,\varphi)$. Each particle is characterized by its own holding potential, which depends on the relative position of neighbor particles and the type of interaction forces (e.g., hard contacts, electrostatic, and Van der Waals). Given the disordered nature of sediment, this potential possesses local minima corresponding to a certain number of random, or almost random orientations at equilibrium.

Small perturbations produce reversible particle rotation within the potential wells of U, which determine the elastic response of sediment. Larger perturbations, on the other hand, might be sufficient to overcome the potential barriers between local minima, in which case irreversible particle rotation will occur, yielding plastic deformations. Especially for irreversible rotations, holding potentials change in response to relative particle displacement/rotation, so that a rigorous formulation of $U(\theta,\varphi)$ must take the time evolution of particle interactions into account. Because details about such interactions are largely unknown, we proceed with a simplified approach based on static random potentials. These potentials can reproduce the fundamental difference between sediment and diluted suspensions, i.e., the existence of forces that must be overcome in order to irreversibly change particle orientations. Holding potentials are ultimately responsible for blocking remanence carriers against changes of the ambient field and, in the laboratory, against applied fields, for instance during alternating field (AF) demagnetization.

As seen in section 3.1, solutions of the Smoluchowski-Debye equation for the statistical distribution $p(\theta,\varphi)$ of particle orientations at equilibrium are governed by the total potential of each particle, which is now

given by $V_i = -m_i B\cos\theta + U_i(\theta,\varphi)$ for particle i. Because each particle is subjected to its own holding potential, $p(\theta,\varphi)$ is the ensemble average of single particle solutions, i.e.,

$$p(\theta,\varphi) = \left\langle c_i \exp\left(\frac{m_i B\cos\theta - U_i(\theta,\varphi)}{D_r\Gamma_r}\right)\right\rangle, \tag{13}$$

where $\langle\ldots\rangle$ is used to indicate an ensemble average. $D_r\Gamma_r$ is conveniently replaced by the amplitude τ_p of randomizing torques. In order to evaluate equation (13), we need an explicit formulation of U_i as a random potential with an appropriate number of local minima representing stable orientations in the force field caused by neighbor particles. For this purpose, we follow the general solution approach of *Alexiewicz* [2000] and represent U_i as a series of spherical harmonic functions, i.e.,

$$U_i(\theta,\varphi) = \sum_{l,m} u_l(\xi_{i,m}\cos m\varphi + \zeta_{i,m}\sin m\varphi)P_l^m(\cos\theta), \tag{14}$$

where P_l^m are the associated Legendre polynomials with Schmidt quasinormalization [*Winch et al*., 2005], u_l are coefficients expressing the expected spectral amplitude of terms with order l, and $\xi_{i,m}$, $\zeta_{i,m}$ are random realizations of a statistical variable with zero expectation, unit variance, and a given probability density function, e.g., the normal distribution $\boldsymbol{N}(0,1)$. The spectral amplitudes u_l should be chosen so that the number of local minima is comprised between 2 (i.e., uniaxial holding potentials) and the maximum number ($\sim$10) [*Torquato*, 1995] of nearest random packing neighbors. Furthermore, the associated torques $\mathbf{T}_i = -\nabla U_i$ shall be characterized by a white spherical harmonic spectrum. These conditions can be satisfied only if the sum in equation (14) is truncated to a certain maximum harmonic degree n. In this case,

$$U_i(\theta,\varphi) = \left[\sum_{l=1}^{n}\frac{l}{2l+1}\right]^{-1/2}\sum_{l=1}^{n}\frac{1}{\sqrt{(l+1)(2l+1)}}\sum_{m=0}^{l}(\xi_{i,m}\cos m\varphi + \zeta_{i,m}\sin m\varphi)P_l^m(\cos\theta) \tag{15}$$

yields unit root mean square torques, i.e., $\langle T_i^2\rangle = 1$ (see supporting information S3 for a proof based on *Constable and Parker* [1998]). Some realizations of U_i with $n = 4, 6, 9$ are shown in Figure 3.

The ensemble average of equation (13) with U_i given by equation (15) yields the mean equilibrium magnetization

$$\frac{M_{eq}}{M_0} = \left\langle \frac{1}{p_{0,i}}\int\int_{\Omega}\exp\left(\frac{m_i B}{\tau_p}\cos\theta - \frac{\tau_h}{\tau_p}U_i(\theta,\varphi)\right)\sin\theta\cos\theta\,d\theta\,d\varphi\right\rangle, \tag{16}$$

where Ω denotes integration over the unit sphere, and τ_p, τ_h are the root mean square amplitudes of perturbing and holding torques acting on individual particles, respectively.

Equation (16) cannot be evaluated analytically; however, the main characteristics of the equilibrium magnetization can be understood by considering two limit cases. The first limit case is that of a weak holding potential, i.e., $\tau_h \ll \tau_p$, which means that particles are practically free to rotate under the influence of perturbing torques, yielding the Langevin law in equation (12). For strong holding forces, i.e., $\tau_h \gg \tau_p$, the orientation of individual particles is dictated by local, randomly positioned minima of U_i. Such orientations deviate from the equilibrium resulting from the interplay between magnetic and perturbing forces, thereby reducing the overall alignment with the applied field (Figure 4a). In practice, the Langevin approximation obtained by neglecting the holding potential is valid for $\tau_h/\tau_p < 1$ (Figure 4b). Above this limit, M_{eq}/M_0 starts to decrease with increasing τ_h, i.e.,

$$\frac{M_{eq}}{M_0} \approx \boldsymbol{L}\left(q\frac{mB}{\tau_h}\right), \tag{17}$$

where q is a constant that depends weakly on the maximum order n of the spherical harmonics used to construct the random holding potentials (i.e., $q \approx 3.0, 3.9, 4.9$ for $n = 4, 6, 9$, respectively). Finally, a general analytical approximation of equation (16) that holds for both limit cases as well as intermediate solutions is given by (Figure 4b)

$$\frac{M_{eq}}{M_0} \approx \boldsymbol{L}\left(\frac{mB}{\sqrt{\tau_p^2 + (\tau_h/q)^2}}\right). \tag{18}$$

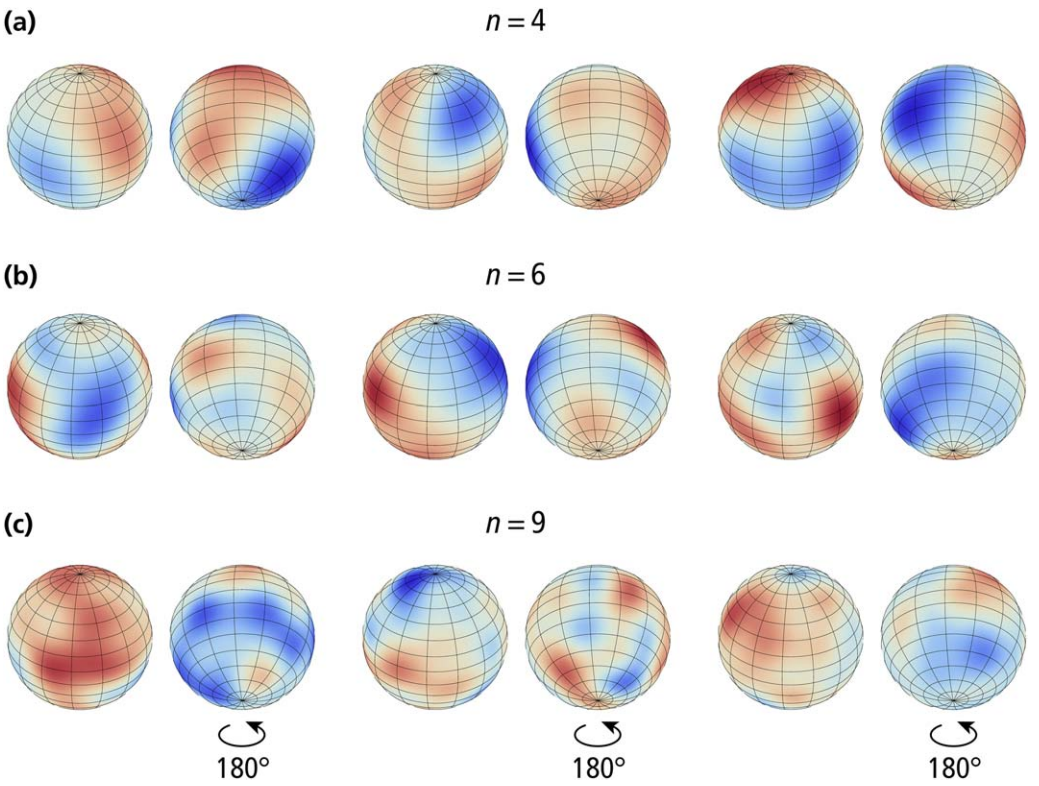

Figure 3. Examples of random holding potentials $U(\theta, \varphi)$ generated with equation (15) using spherical harmonic functions with maximum degree (a) $n=4$, (b) $n=6$, and (c) $n=9$. Three examples are given for each n, with the right-hand image showing the same potential as the left-hand one after 180° rotation. Stable particle orientations are defined by local minima of $U(\theta, \varphi)$ (blue).

In this case, $q \approx 1.31\, n^{0.6}$ is the value of the "Boltzmann factor" $\beta_h = \tau_h/\tau_p$ for which the equilibrium MRM attained in small fields is $2^{-1/2} \approx 71\%$ of the value predicted by the Langevin law in absence of holding forces. If $mB \ll \tau_p$, as expected inside the mixed layer (see section 4), a linear approximation of equation (18) based on $\boldsymbol{L}(x) \approx x/3$ yields

$$\frac{M_{eq}}{M_0} \approx \frac{mB}{3\sqrt{\tau_p^2 + (\tau_h/q)^2}}. \tag{19}$$

An important effect of the holding potential, beside that of lowering the equilibrium MRM, consists in slowing down the rate at which this equilibrium is approached: as τ_h becomes larger than τ_p, fewer perturbations are able to overcome the energy barriers of U_i to produce irreversible magnetic moment rotations, until the system becomes entirely fixed for $\tau_h \gg \tau_p$. This effect plays a fundamental role in locking the acquired MRM at the bottom of the mixed layer, as explained in section 4.

3.3. Inclination Shallowing

Sediment NRM is often affected by inclination shallowing, due to rotation of elongated magnetic grains toward horizontal directions [*Griffiths et al*., 1960; *Mitra and Tauxe*, 2009; *Jezek et al*., 2012] and to sediment compaction [*Arason and Levi*, 1990]. While compaction-shallowing occurs at depths of several tens of meters below the mixed layer and is not relevant for initial NRM acquisition, a possible MRM shallowing source is represented by sediment texture. Sediment texture is typically produced by the preferred horizontal layering of platy particles (e.g., clay). Although texture buildup inside the mixed layer is counteracted by mixing, a certain degree of mechanical anisotropy can be expected in clay-rich sediment. Direct measurements of mechanical strength anisotropies are not available for the mixed layer; however, an upper limit can be deduced from data for pure clays, where the relative shear strength anisotropy is usually comprised between 20 and 60% with an average of ~40% [*Won*, 2013].

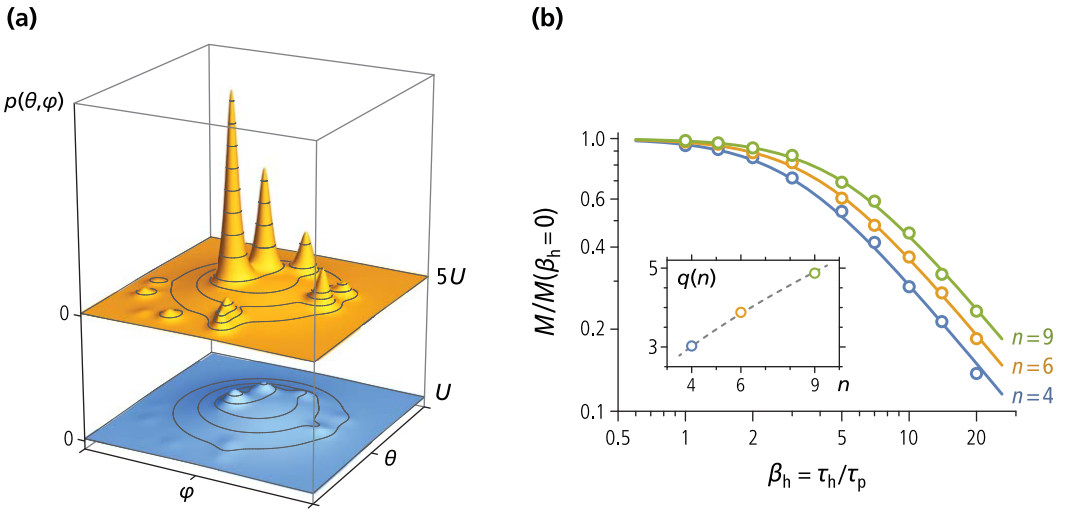

Figure 4. (a) Probability density function $p(\theta, \varphi)$ of particle orientation in a total potential $-mB+U$ (blue surface) and $-mB+5U$ (orange surface), where U is a random holding potential. Local minima of U produce probability maxima at random orientations (peaks) that do generally not coincide with the direction (θ_0, φ_0) of B. This effect is particularly pronounced for large amplitudes of U (orange surface), resulting in smaller mean particle alignments and equilibrium magnetizations. (b) Decrease of the equilibrium magnetization M in random holding potentials of the type shown in Figure 3, with respect to the case of no holding potential (i.e., $\beta_h=0$). Each dot corresponds to the ensemble average of up to 3×10^5 random potential realizations with maximum spherical harmonic order $n=4, 6, 9$. Lines are least squares fits of the numerical results according to equation (18). The dependence of the fitting parameter q on n is shown in the inset.

On a microscopic scale, mechanical strength anisotropies are caused by interaction forces with direction-dependent mean amplitudes, which introduce preferred directions for the orientation of nonequidimensional sediment particles. The direction of magnetic moments is affected by this phenomenon only if the following conditions are met simultaneously: (1) magnetic sediment particles are not equidimensional and (2) the corresponding net magnetic moment direction is systematically related to particle shape. Magnetite-clay aggregates [*Galindo-González et al.*, 2009] fulfill these conditions if the magnetic moment of adhering magnetite crystals is parallel to large faces of clay platelets, as is expected for magnetosome chains. Magnetic textures created by this mechanism can be modeled by adding a systematic term A to the random holding potentials, with preferred directions defined by local minima of A. The simplest form for such a potential is given by an uniaxial anisotropy contribution $A=\tau_a\cos(2\theta)/2$, where θ is the angle to the vertical and τ_a is the maximum torque amplitude produced by A. In case of MRM acquisition in inclined fields, the total potential acting on magnetic particles is then given by

$$V(\theta, \varphi)=-mB(\mathbf{n}\cdot\mathbf{b})+\frac{\tau_a}{2}\cos(2\theta)+U_i(\theta, \varphi), \tag{20}$$

where $\mathbf{n}=(\sin\theta\cos\varphi, \sin\theta\sin\varphi, \cos\theta)$ is the unit vector representing the direction of magnetic moments in a field B parallel to the unit vector $\mathbf{b}=(\sin\psi, 0, \cos\psi)$. As seen in section 3.2, random potentials U_i have the effect of dispersing magnetic moments orientations without changing their mean direction. Therefore, U_i can be neglected in inclination shallowing calculations and the mean direction of the acquired MRM is obtained by integration of the Boltzmann distribution associated with equation (20) after setting $U_i=0$, i.e.,

$$\langle\mathbf{n}\rangle \propto \int_0^{2\pi}\int_0^{\pi} e^{\beta_m(\mathbf{n}\cdot\mathbf{b})-\beta_a\cos(2\theta)/2}\,\mathbf{n}\sin\theta\,d\theta\,d\varphi, \tag{21}$$

where $\beta_m=mB/\tau_p$. Furthermore, $\beta_a=\tau_a/\tau_p$ is a new "Boltzmann factor" representing the ratio between anisotropy and perturbing torques. Because $\beta_m \ll 1$ inside the mixed layer, equation (21) can be linearized with respect to β_m and solved analytically (supporting information S4), obtaining the classical inclination shallowing equation

$$\tan I=f_a\tan I_B \tag{22}$$

of *King* [1955], where $I=90^\circ-\theta$ and $I_B=90^\circ-\psi$ are the magnetization and field inclinations, respectively, and

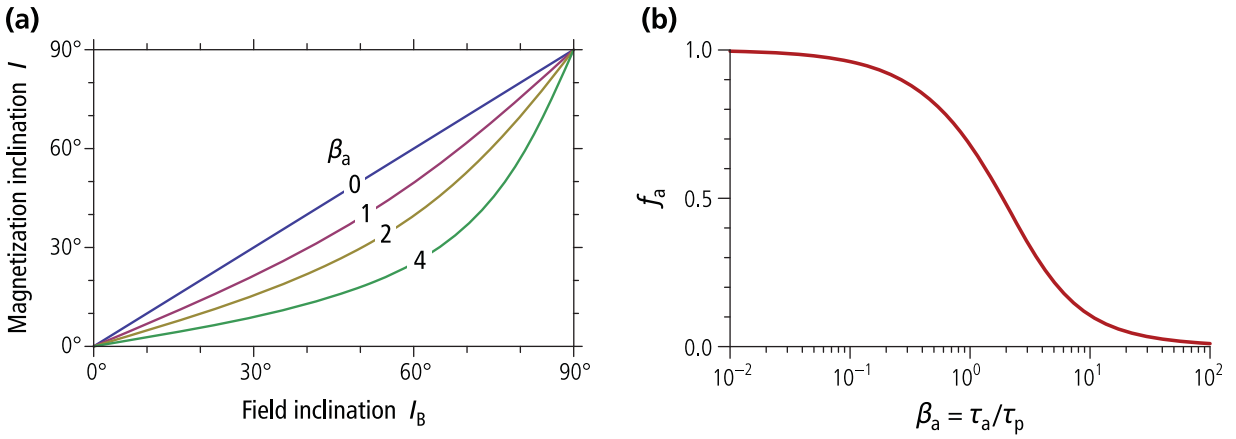

Figure 5. (a) Inclination shallowing of the equilibrium MRM, calculated with equations (22) and (23) for given values of $\beta_a = \tau_a/\tau_p$, which represent increasing amplitudes of the anisotropy term $A = \tau_a \cos(2\theta)/2$ of the holding potential. (b) Inclination shallowing parameter f_a as a function of β_a according to equation (23).

$$f_a = \frac{1 - \sqrt{\frac{\beta_a}{\pi}} \frac{2e^{-\beta_a}}{\operatorname{erf}\sqrt{\beta_a}}}{\beta_a - \frac{1}{2} + \sqrt{\frac{\beta_a}{\pi}} \frac{e^{-\beta_a}}{\operatorname{erf}\sqrt{\beta_a}}} \tag{23}$$

is the inclination shallowing factor associated with the anisotropy potential A (Figure 5a). Maximum inclination shallowing effects observed in nature correspond to $f_a \approx 0.4$ [*Tauxe and Kent*, 2004], which, if associated with a MRM, would require $\beta_a \approx 2.5$ (Figure 5b). On the other hand, if MRM blocking occurs at $\tau_h/\tau_p \approx 1$, as discussed in section 4, β_a is identifiable with the relative anisotropy τ_a/τ_h of holding forces. This anisotropy can be expected to coincide with the relative anisotropy derived from mechanical strength parameters. Assuming $\tau_a/\tau_h \leq 20\%$ for sediments containing up to 50% clay, the maximum MRM inclination shallowing does not exceed 2.3°. Much smaller effects are expected for sediment particles lacking strong shape anisotropies, such as in carbonaceous sediments, where MRM inclination shallowing should be negligible.

4. MRM Acquisition and the Lock-In Function

As seen in section 3, a dynamic equilibrium between ordering forces (i.e., magnetic torques) and randomizing forces (i.e., bioturbation and mechanical interactions) is established inside the surface mixed layer if stationary conditions are maintained for sufficiently long times. The equilibration time depends on the mixing rate of sediment, which decreases with increasing depth, especially near the boundary between mixed and consolidating layers, up to the point where the MRM equilibrium becomes fixed. In the framework of PDRM models, the amount of blocked magnetization is expressed as a function of depth through a so-called lock-in function [*Roberts and Winklhofer*, 2004]. In this section, we model MRM acquisition and its lock-in by following the journey of sediment flocs from the water column to the consolidating layer. For this purpose, we use a coordinate system that moves with the mean sinking (in water) or burial (in the sediment column) velocity $\omega = \mathrm{d}z/\mathrm{d}t$. A thin horizontal layer anchored within this coordinate system will not always contain the same material because of different sinking velocities (in water) and diffusion (in water and sediment). As seen in section 3, rotational diffusion in the presence of magnetic torques and mechanical particle interactions is governed by the Smoluchowski-Debye equation, so that the statistical distribution $p(t, \theta, \varphi)$ of particle orientations inside our layer at any time t is given by

$$\frac{1}{D_r(z'(t))} \frac{\partial p}{\partial t} = \Delta p + \frac{1}{\tau_p(z'(t))} \nabla [p \nabla (-mB \cos\theta + \tau_h(z'(t))\, U)], \tag{24}$$

where $\tau_h U$ is a random potential generating torques with root mean square amplitude τ_h, and τ_p is the root mean square amplitude of random perturbing torques (e.g., turbulence in water and bioturbation in sediment). Furthermore,

$$z'(t)=\frac{z(t)}{L}=\frac{1}{L}\int_0^t \omega(z')\,dt \tag{25}$$

is the reduced depth of our layer as a function of time, and D_r, ω, τ_p, and τ_h are assumed to be steady state sediment properties that depend only on the reduced depth $z'=z/L$, where L is the thickness of the mixed layer.

A general analytical expression for the time-dependent solution of equations (24) and (25) is not known; therefore, we proceed with some simplifications. The first simplification consists in assuming ω to be a constant, in which case equation (25) reduces to $z'=\omega t/L$. Next, we neglect all potentials and look for a general solution of the (time-dependent) diffusion equation

$$\frac{\partial p}{\partial t}=D_r(\omega t/L)\,\Delta p, \tag{26}$$

which describes the fate of a given magnetization in zero field over time. As far as the effect of potentials on the preservation of remanent magnetizations is concerned, the reduced probability for successful irreversible rotations against strong holding torques (section 3.2) is equivalent to a decrease of D_r, as we will be shown below. Before proceeding to solve equation (26), we need to specify the dependence of the rotational diffusion constant D_r on depth, assuming that it is entirely caused by bioturbation. Available estimates of the biodiffusion constant (D_b) are generally given as bulk averages over the mixed layer. As discussed by *Reed et al*. [2006], reconstructions of $D_b(z')$ from tracer dynamics require assumptions about the bioturbation mechanism, with possible solutions ranging from nearly depth-independent functions to a Gaussian-like decrease of $D_b(z')$ when moving down from the sediment-water interface. The latter model is considered more realistic, because D_b is expected to depend on the concentration of benthic organisms, and therefore on nutrient concentration profiles dictated by organic matter consumption [*Rabouille and Gaillard*, 1991; *Boudreau*, 1998; *Reed et al*., 2006].

Generally, organic carbon concentrations decrease exponentially within the mixed layer, down to levels that no longer support the energetic costs of deep burrowing [*Berner*, 1980; *Rabouille and Gaillard*, 1991; *Roberts and Winklhofer*, 2004]. Therefore, we assume that the concentration of motile benthic organisms responsible for bioturbation is proportional to the exponential decrease of organic carbon content with depth. Accordingly, the simplest bioturbation model assumes D_b and D_r to be proportional to exponential-like organic carbon profiles, i.e., $D_r=D_{r,0}c_b(z')$ where $D_{r,0}$ is the maximum value of D_r (typically at the top $z=0$ of the sedimentary column) and $c_b(z')$ is an exponential profile with $c_b(0)=1$, e.g., $c_b(z')=e^{-3z'}$ (Figure 6b). Additional factors that affect D_r are (1) species-dependent biological limits, for example, burrowing depths, and (2) the reduced probability of irreversible particle rotation as the mechanical strength of sediment (i.e., τ_h) increases. These two factors are somewhat connected because motile organisms will not thrive where their activity is severely limited by the mechanical strength of sediment.

Limitation of D_r by sediment resistance is quantified by the probability for random perturbations (i.e., torques with amplitude τ_p) to overcome the energy barriers of the holding potential $\tau_h U$. This situation is equivalent to that of thermal activations, where the probability of thermal perturbations with energy $k_B T$ to overcome a given energy barrier ΔE is expressed by the Arrhenius law $e^{-\Delta E/k_B T}$. Mean energy barriers of the holding potential are dictated by the typical excursions of $\tau_h U(\theta,\varphi)$ over the unit sphere, which coincide with τ_h. In this case, the probability of irreversible particle rotations is given by $e^{-\tau_h/\tau_p}$ and our model for the rotational diffusion constant becomes

$$D_r=D_{r,0}c_b(z')\,e^{-\beta_h(z')}, \tag{27}$$

with $\beta_h(z')=\tau_h/\tau_p$. Lacking specific information on bioturbation forces, we assume that τ_p (i.e., the driving "force" of bioturbation) is a constant, while τ_h increases with depth because of sediment compaction. As a last step of our model construction, we need a reasonable estimate of $\tau_h(z')$. Since displacement of benthic organisms is attributed to crack propagation [*Dorgan et al*., 2006], we assume τ_h to be proportional to the tensile fracture toughness K_{IC} of sediment, and we use profiles of this parameter measured by *Johnson et al*. [2012] to construct the depth dependence of β_h. These profiles are characterized by a continuous increase of $K_{IC}(z)$ with a kink and at the bottom $z=L$ of the mixed layer that marks the onset of consolidation (Figure 6a). The nearly linear dependence of K_{IC} on depth within the mixed layer can be attributed mainly to compaction. Similar profiles are also seen with shear strength measurements [*Locat et al*., 2002].

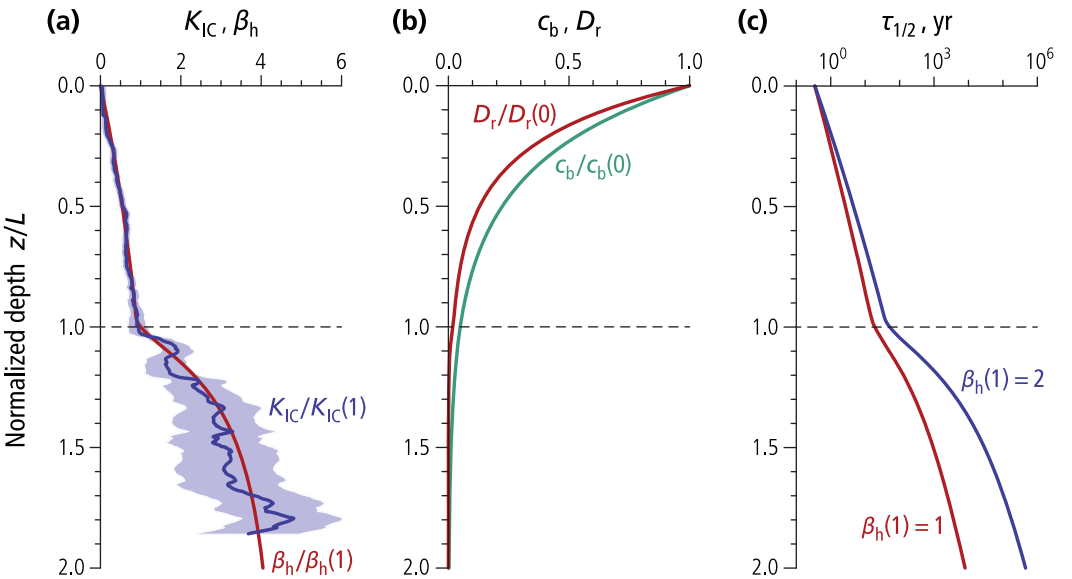

Figure 6. Typical sediment property profiles relevant for DRM preservation and MRM acquisition. (a) Sediment strength, expressed as the ratio $\beta_h = \tau_h/\tau_p$ between root mean square amplitudes of holding torques, τ_h, and perturbing torques, τ_p (red line). Perturbing torque amplitudes are assumed to be independent of sediment depth, while τ_h is assumed to be proportional to tensile fracture toughness (K_{IC}) profiles measured in marine sediment (from data in *Johnson et al.* [2012]). The average (blue line) of three K_{IC} profiles with double standard deviation confidence band (shaded) is shown after normalization with respect to sediment depth and amplitude in order to obtain a unit value at the bottom of the mixed layer (dashed line), so that $\beta_0 = \beta_h(L) = 1$. (b) Normalized profiles of benthic organism concentration c_b and rotational diffusion D_r according to equation (27). (c) Equilibration half-time $\tau_{1/2}$ of mixed-layer magnetizations, calculated on the basis of properties shown in Figures 6a and 6b. Two β_h profiles proportional to Figure 6a have been chosen. Note the logarithmic time axis in Figure 6c.

From a rheological point of view, continuous shear associated with bioturbation is expected to reduce the shear strength (a phenomenon known as shear thinning, e.g., *Barnes* [1997]). On the other hand, benthic organisms can excrete gelation substances that produce the opposite effect. Indeed, mixed results have been found upon adding selected species of burrowing organisms [*Meadows and Tait*, 1989]. Therefore, we avoid explicit links between β_h and the concentration c_b of benthic organisms, and define $\beta_h(z')$ as proportional to the K_{IC} profiles of *Johnson et al.* [2012], with absolute values determined by $\beta_0 = \beta(1)$ (Figure 6a). In the absence of direct β_h estimates, we assume that the bottom of the mixed layer corresponds to places where bioturbation becomes increasingly difficult because of holding forces that exceed the driving forces of bioturbation. This criterion is equivalent to setting $\beta_0 \geq 1$. Our model for $D_r(z)$ uses a minimum set of reasonable assumptions about bioturbation and mechanical sediment properties, yielding a pseudoexponential profile of D_r through the mixed layer (Figure 6b), which is similar to D_b profiles assumed elsewhere [e.g., *Bentley et al.*, 2006].

The time evolution of the remanent magnetization of a sediment layer initially located at a depth z_0 below the sediment-water interface is obtained from equation (26) with the initial condition $p(\theta, t=0)$ corresponding to a given value M_{ini} of M. Any initial distribution p of the form given by equation (4) yields the same normalized solution $M(t)/M_{ini}$. Because the layer moves down with respect to the sediment-water interface, this solution can be converted into a depth profile through $z = z_0 + \omega t$, obtaining (supporting information S5)

$$\frac{M(z, z_0)}{M_{ini}} = \exp\left[-2\frac{L}{\omega}\int_{z_0/L}^{z/L} D_r(u)\,du\right]. \tag{28}$$

If D_r from equation (27) is substituted into this solution, initial magnetizations decay more or less rapidly to zero or to a constant value, depending on the starting depth z_0 (Figure 7a). Magnetization decays are more rapid near the top of the sediment column, where D_r is maximal, and slow down as the consolidating layer is approached. A common characteristic of all solutions is that $M(z, z_0)$ becomes constant below a certain "full blocking" depth $z_B > L$ inside the consolidating layer. Magnetizations $M(z_B, z_0)$ at this depth represent

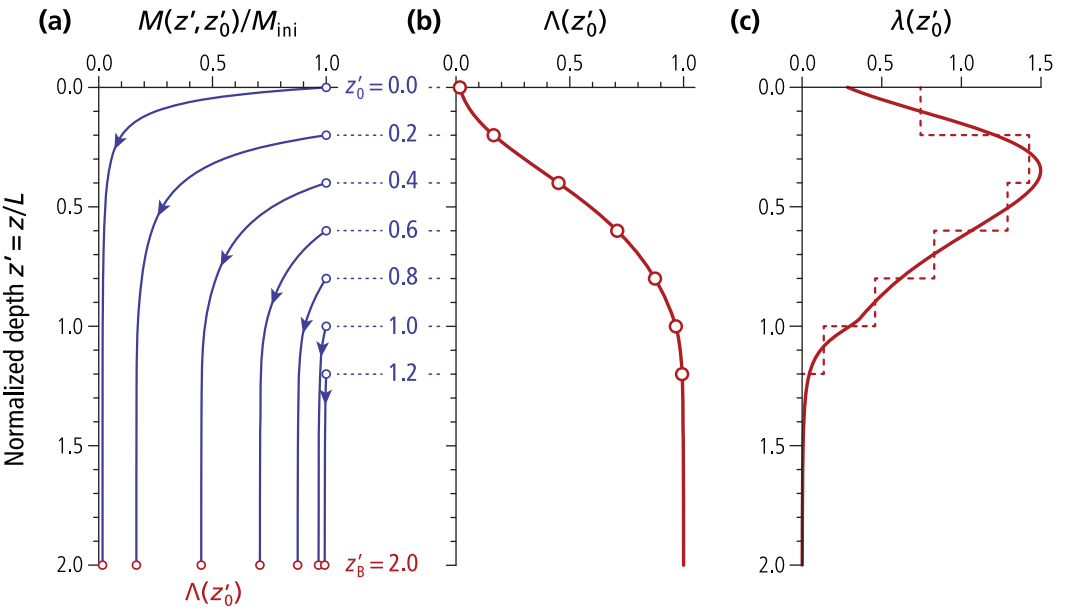

Figure 7. Illustration of the MRM lock-in process. (a) Evolution of normalized initial magnetizations acquired at different depths z'_0 (blue dots), as the corresponding sediment layer gets buried (lines). All magnetizations converge to constant values at depths $z' > z'_B = 2$ (red dots). These values define the lock-in function $\Lambda(z'_0) = M(z'_B, z'_0)$ shown in Figure 7b. The particular case $M(z'_B, z'_0 = 0)$ corresponds to the DRM fraction that survives its journey through the mixed layer. (b) Lock-in function deduced from Figure 7a. (c) First derivative $\lambda(z'_0)$ of the lock-in function (solid line), which defines the relative contribution of each depth to the final magnetization. The dashed line represents magnetizations corresponding to differences between curves in Figure 7a.

fractions of the initial magnetizations acquired at z_0 that survived the journey though the mixed layer. These fractions yield, by definition, the MRM lock-in function

$$\Lambda(z') = \exp\left[-2\frac{L}{\omega}\int_{z'}^{z'_B} D_r(u)\,du\right], \tag{29}$$

where $z'_B = z_B/L$ (Figure 7b). Unlike most definitions of the lock-in function commonly used in PDRM models, $\Lambda(z')$ does not start inside the consolidating layer. Instead, it is defined for all depths below the sediment-water interface, as proposed by *Channell and Guyodo* [2004]. The reason for such a wide lock-in function is that magnetizations acquired inside the mixed layer can be preserved. Moreover, it is possible for a DRM, which in our model is equivalent to $M(0, z_0 = 0)$, to be partially preserved (i.e., $M(z_B, z_0 = 0) > 0$) for some combinations of D_r, L, and ω (Figure 7a), in accordance with our preliminary estimates in section 2. In this case, the lock-in function is characterized by $\Lambda > 0$ at the sediment-water interface, and small lock-in depths can result in combination with the minimal mixing depths (e.g., $L \approx 2$ cm) encountered in some pelagic sediments [*Tauxe et al*., 2006].

The last element of our MRM acquisition model provides an estimate of the MRM intensity that is ultimately locked inside the consolidating layer, as discussed in the following. For this purpose, we define the lock-in probability density $\lambda(z')$ as the derivative of $\Lambda(z')$ with respect to z' (Figure 7c). Accordingly, $\lambda(z')\,M_{eq}(z')$ represents the relative contribution to the locked MRM that is delivered by the equilibrium remanence, $M_{eq}(z')$, acquired inside a layer of thickness dz at depth z, as specified by equation (18). The total NRM is therefore obtained by integration of $\lambda(z')\,M_{eq}(z')$ over z', i.e.,

$$\frac{M_{NRM}}{M_0} = \Lambda(0)\frac{M_{DRM}}{M_0} + \int_0^{z'_B} \lambda(z')\frac{M_{eq}(z')}{M_0}\,dz', \tag{30}$$

where $\Lambda(0)M_{DRM}$ is the DRM fraction that survives burial through the mixed layer. Using the result derived in section 3 for the equilibrium MRM we finally obtain the chief result of this paper, i.e.,

$$\frac{M_{NRM}}{M_0} = \Lambda(0)\frac{M_{DRM}}{M_0} + \frac{M_{MRM}}{M_0}, \tag{31}$$

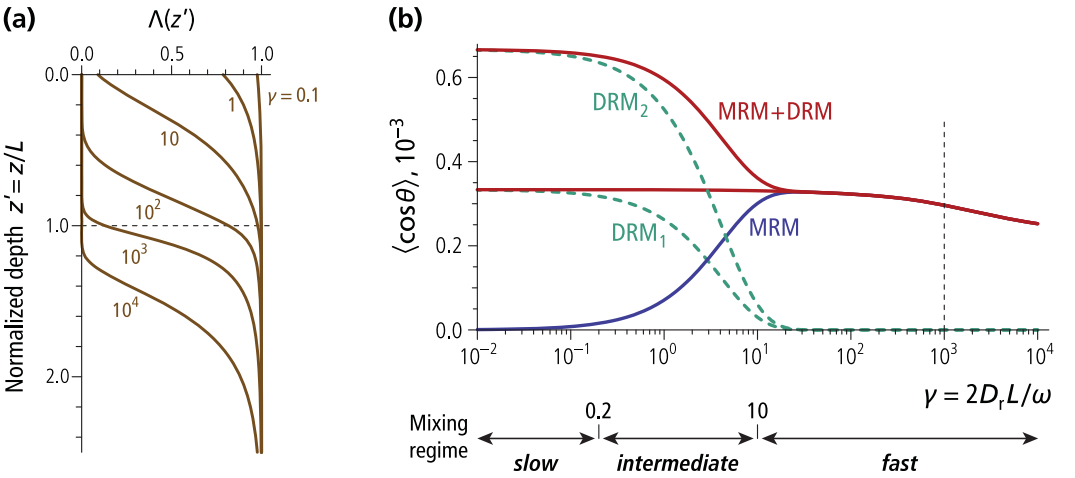

Figure 8. Lock-in functions and remanent magnetizations acquired in a sediment with properties shown in Figure 6 and $\beta_m = 10^{-3}$ (i.e., acquisition in a 50 μT field when the mean amplitude τ_h of holding and perturbing torques at the bottom of the mixed layer is equal to the torque exerted by a 50 mT field). (a) Lock-in functions $\Lambda(z')$ for selected values of the rotational diffusivity parameter $\gamma = 2D_r L/\omega$. The value $\Lambda(0)$ of the lock-in function at the sediment-water interface yields the fraction of locked-in DRM. The bottom of the mixed layer is marked by the dashed line. (b) Finally locked DRM and MRM as a function of γ for two DRM settings, i.e., DRM_1 acquired with same perturbation strength as MRM (i.e., $\tau_{p,DRM} = \tau_{p,MRM}$) and the more realistic DRM_2 acquired in a less perturbed environment (i.e., $\tau_{p,DRM} = 0.5\,\tau_{p,MRM}$). Three mixing regimes yielding full, intermediate, and no DRM preservation, respectively, are shown below. The vertical dashed line marks the limit above which lock-in starts below the mixed layer.

where the MRM lock-in function is given by (Figure 8a)

$$\Lambda(z') = \exp\left[-\gamma \int_{z'}^{z'_B} c_b(u)\, e^{-\beta_h(u)}\, du\right], \tag{32}$$

and the acquired MRM is given by

$$\frac{M_{MRM}}{M_0} = \gamma \int_0^{z'_B} \Lambda c_b e^{-\beta_h} \boldsymbol{L}\left(\frac{mB}{\tau_p}\frac{1}{\sqrt{1+(\beta_h/q)^2}}\right) dz', \tag{33}$$

where $\gamma = 2D_0 L/\omega$ is the rotational diffusivity parameter of the mixed layer introduced in section 2. The first and second term on the right-hand side of equation (31) are the DRM and MRM contributions to the acquired NRM, respectively. Both terms are functions of γ, whose unit is rad^2. This parameter represents the mean squared angle of a random walk produced by rotational diffusion during the typical residence time of sediment particles within the mixed layer. DRM preservation is only possible with $\gamma < 1$, while full MRM acquisition with complete DRM obliteration is obtained with $\gamma \gg 1$.

Numerical evaluations of equations (31–33) reveal that a transition from a DRM-dominated to a MRM-dominated NRM occurs between $\gamma = 0.2$ and $\gamma = 10$ (Figure 8). Accordingly, we define three regimes of sedimentary NRM acquisition: (1) a slow mixing regime for $\gamma \leq 0.2$, where the preserved magnetization is essentially a DRM, (2) a fast mixing regime for $\gamma \geq 10$, where DRM is fully randomized and replaced by a MRM, and (3) an intermediate mixing regime with $0.2 < \gamma < 10$, where DRM and MRM coexist, both contributing to a total NRM. Faster sediment mixing regimes push the MRM lock-in function below the mixed layer (Figure 8a), where the biodiffusion rate declines rapidly, producing large lock-in depths that are compatible with some paleomagnetic records [e.g., *Sagnotti et al.*, 2005; *Suganuma et al.*, 2011].

Because DRM and MRM are characterized by different acquisition efficiencies, total NRM intensities can be particularly sensitive to γ in case of intermediate mixing regimes, due to varying DRM and MRM proportions. On the other hand, MRM intensity is relatively insensitive to mechanical sediment properties (i.e., β_h in Figures 9a and 9b) and bioturbation parameters (i.e., c_b in Figures 9c and 9d), especially for fast mixing regimes. Moreover, the total magnetization is governed only by the ratio between magnetic and perturbing torques for mixing regimes characterized by $20 < \gamma < 500$, according to the limit case of equation (19) with $\tau_h \to 0$.

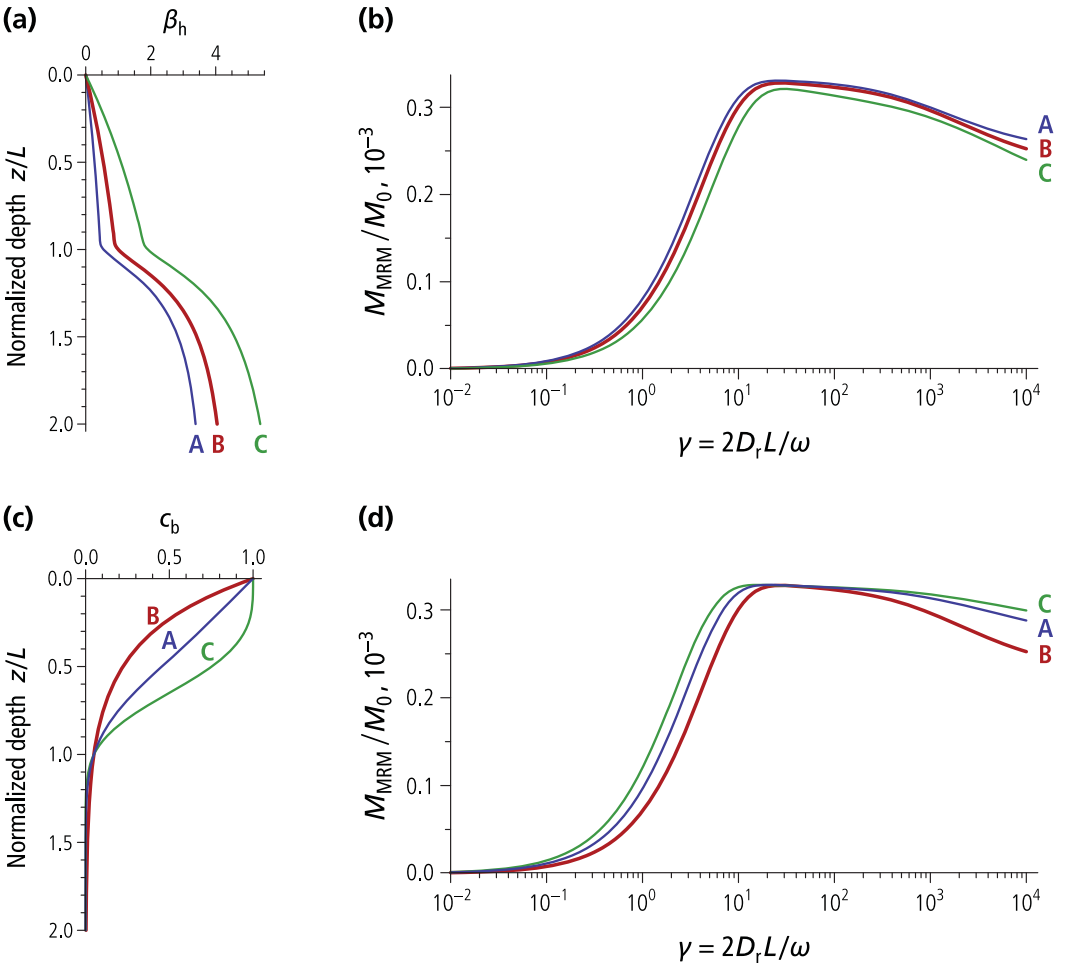

Figure 9. Sensitivity of MRM acquisition to variations of the model profiles shown in Figure 6. (a) Sediment strength variations, expressed by proportional β_h profiles with $\beta_h(1)=0.5$ (case A), $\beta_h(1)=1$ (case B as in Figure 6a), and $\beta_h(1)=2$ (case C). (b) MRM intensities that correspond to the cases shown in Figure 9a. (c) Variations of normalized concentration profiles c_b of benthic organisms according to an exponential model (case B as in Figure 6b), a more box-shaped function (case C), and an intermediate case (case A). (d) MRM intensities that correspond to the cases in Figure 9c. MRM intensities depend only weakly on variations of the profiles shown in Figures 9a and 9c, especially in case of fast mixing regimes with $20 \leq \gamma \leq 500$.

5. Discussion

In sections 3 and 4, we derived equations that describe the mean alignment of magnetic particles subjected to the simultaneous action of aligning torques (i.e., magnetic and texture) and randomizing torques (i.e., turbulence, bioturbation, and interparticle mechanical interactions). DRM and MRM acquisition depend on the mean intensity of such torques and on the frequency of "successful" perturbations inside the corresponding environments (i.e., water column, sediment-water interface, and mixed layer). Dynamic equilibrium between the above mentioned torques is described by a Langevin law of the type $M_{eq}=M_0\boldsymbol{L}(\beta_m)$, where M_0 is the magnetization of fully aligned magnetic moments, and the "Boltzmann factor" $\beta_m=\tau_m/\tau_p$ is the ratio between the amplitudes of magnetic torques, $\tau_m=mB$, and perturbing torques, τ_p. Two main cases can be distinguished according to the nature of perturbing torques. In the first case, magnetic moments are carried by discrete units (i.e., flocs) with few reciprocal interactions. While falling inside the water column, magnetic flocs are subjected to Brownian perturbations, as well as hydrodynamic disturbances produced by turbulence [*Heslop*, 2007]. The typical intensity of such disturbances yields relatively large values of β_m, which produce the well-known problem of nonlinear DRM field dependencies [e.g., *Tauxe et al.*, 2006]. This problem is mitigated by accretion of large (>20 μm) flocs through random aggregation of smaller units.

Floc density increases dramatically at the sediment-water interface, where a network of interaction forces begins to form. The physics of DRM acquisition remains the same as long as individual flocs behave as independent units with few interactions. Perturbing forces are presumably larger than in the water column, due to sediment resuspension by benthic organisms and continuous floc reorientation in a turbulent hydrodynamic regime (Figure 1). In most cases, sediment mixing is expected to be fast enough to expose all materials inside the mixed layer to repeated resuspension events and DRM renewal. Under these conditions, new magnetic carriers formed inside the mixed layer, such as magnetosome chains, acquire the same type of NRM as older carriers, and are subjected to the same lock-in delay. This is confirmed by results of *Ouyang et al*. [2014], who did not find a systematic time lag between detrital and biogenic NRM components in paleointensity records from the South China Sea.

Interaction forces between sediment particles grow rapidly below the sediment-water interface, as soon as a sufficient number of contact points is reached. In this case, individual magnetic flocs are no longer independent units, and, in the absence of perturbations, the orientation of magnetic moments becomes locked, yielding a stable remanent magnetization. Bioturbation, however, produces irreversible particle rotations by overcoming the holding forces. Flocs are expected to break into smaller units whose internal binding forces exceed those produced by bioturbation. Such units might be identified with the "fundamental flocs" assumed in some DRM models [e.g., *Tauxe et al*., 2006]. As far as magnetofossils are concerned, fundamental flocs might consist of magnetosome chains adhering to clay particles, as postulated by *Mao et al*. [2014a]. We have modeled bioturbation by the action of perturbing torques, τ_p, against so-called holding potentials. The amplitude of τ_p depends on a detailed representation of bioturbation mechanisms [e.g., *Dorgan et al*., 2006]; nevertheless, opposing torques, τ_h, caused by interparticle forces must be overcome for successful displacement of living organisms. Therefore, $\beta_h = \tau_h/\tau_p \approx 1$ can be reasonably assumed at the bottom of the mixed layer, where τ_h is also responsible for preservation of a remanent magnetization against the torques resulting from the application of (large) magnetic fields. A crude estimate of torques produced by bioturbation can be derived from $\tau_h/\tau_p \approx 1$ and critical fields B_h required to produce irreversible magnetic moment rotation in fresh sediment samples taken from the bottom of the surface mixed layer. In this case, the "Boltzmann factor" $\beta_m = mB/\tau_p$ is simply given by B/B_h, where B is the field in which NRM was acquired. Using $B_h > 20$ mT as a representative value for the mixed layer [*Mao et al*., 2014a], one obtains $\beta_m < 2.5 \times 10^{-3}$ for typical geomagnetic field intensities. In this case, we expect the intensity of magnetizations acquired inside the mixed layer to be proportional to the geomagnetic field.

The time required for any magnetization to reach full equilibrium with the ambient field inside the mixed layer is inversely proportional to the rotational diffusion constant D_r associated with bioturbation. Direct measurements of D_r are not available, and estimates based on total diffusion are extremely difficult to obtain, due to the unknown efficiency of benthic organisms in inducing irreversible particle rotations. We attempted crude lower limit estimates of D_r on the basis of microbial abundances [*Kallmeyer et al*., 2012], relying on the assumption that the translational and rotational diffusion of microbes is of the same type as for the well-known case of Brownian motion (Table 1). With such estimates, equilibration times are comprised between 30 yr and 30 kyr, depending on the sedimentary setting. The fate of a DRM is dictated by D_r and by the typical residence time L/ω of sediment particles inside a mixed layer of thickness L, which are collectively summarized by the so-called mixed layer diffusivity parameter $\gamma = D_r L/\omega$, where ω is the sedimentation rate. Three mixing regimes can be distinguished on the basis of γ, i.e., (1) slow mixing ($\gamma \leq 0.2$) that leads to full DRM preservation, (2) fast mixing ($\gamma > 10$) during which DRM is completely replaced by a MRM, and (3) intermediate mixing where NRM is a mixture of DRM and MRM (Figure 8b). According to our calculations, inclination shallowing is not expected for MRMs acquired in the fast mixing regime.

Since MRM is essentially a particular type of PDRM, its conversion to a stable NRM depends on a so-called lock-in function, which represents the relative contribution of each depth below the sediment-water interface to the final magnetization. The value of the lock-in function at the sediment-water interface represents the DRM fraction that survives sediment mixing. Lock-in functions associated with slow mixing regimes (e.g., Figure 8a with $\gamma < 10$) are representative of pelagic environments with low nutrient inputs, shallow mixed layers ($L \approx 2$ cm), and small lock-in depths of the order of 1 cm, as postulated by *Tauxe et al*. [2006]. On the other hand, nonzero values of the lock-in function are confined below the mixed layer in case of rapid mixing regimes, yielding typical lock-in depths of $\sim 2L \approx 20$ cm (e.g., Figure 8a with $\gamma > 1000$). These lock-in depths are compatible with estimates obtained from paleomagnetic records by *Suganuma et al*. [2011]. Because of

the strong sensitivity of the lock-in function to mixing regimes, acquired MRM intensities depend mainly on γ, increasing from 0 for slow mixing to the equilibrium magnetization $M_0\boldsymbol{L}(\beta_m)$ for rapid mixing. Numerical MRM intensity estimates can be compared with the NRM of magnetofossil-bearing sediments characterized by rapid mixing regimes. Because of the excellent dispersion of intact magnetofossil chains, with estimated mean distances >9 times the chain length [*Ludwig et al*., 2013], magnetic flocs probably contain a single magnetosome chain or chain bundle with maximum magnetic moment [*Hanzlik et al*., 2002], as inherited from living cells. In this case $M_0 \approx M_s$ can be assumed, and using $M_{rs}/M_s \approx 0.4$ [e.g., *Ludwig et al*., 2013; *Mao et al*., 2014a], we deduce $\mathrm{MRM}/M_{rs} \approx (7\text{-}9)\times10^{-4}$ for $20 \leq \gamma \leq 1000$ (Figure 8b). This estimate agrees well with representative NRM values of magnetofossil-bearing platform carbonates [*McNeill and Kirschvink*, 1993].

Our analysis of DRM and MRM acquisition enables a first discussion of the sensitivity of relative paleointensity records to fluctuations of the NRM acquisition efficiency. With few exceptions associated with extremely rapid accumulation of nutrient-poor sediment material (e.g., ice rafting), bioturbation is sufficiently active to expose the whole mixed layer to repeated resuspension and redeposition events, so that DRM and MRM can be assumed to be carried by the same kind of magnetic particles. Fluctuations of NRM acquisition efficiency in terms of (nonmeasurable) magnetic moment alignments are, therefore, entirely due to the acquisition mechanism. As discussed above, equilibrium DRM and MRM intensities are mainly controlled by β_m, with major differences being related to the intensity τ_p of random perturbations. In both cases, τ_p is mainly controlled by the action of benthic organisms, but not by their concentrations. This means that major changes in the type of benthic fauna are required to introduce significant modifications of resuspension (for DRM) and bioturbation (for MRM) mechanisms. On the other hand, the concentration of benthic organisms is directly proportional to D_r and controls the timing of DRM randomization and MRM acquisition inside the mixed layer. Therefore, moderate fluctuations of the sedimentary environment are expected to change γ through variations of benthic biomass and sedimentation rate. As long as these variations occur around a slow ($\gamma \leq 0.2$) or fast ($\gamma > 10$) mean mixing regime, NRM is controlled either by a DRM or a MRM with nearly constant acquisition efficiency and can be expected to support reliable paleointensity reconstructions. On the other hand, fluctuations of intermediate mixing regimes produce variations in the relative contributions of DRM and MRM. DRM is more efficient than MRM; therefore, the net result is that NRM acquisition efficiency changes in a way that could be erroneously attributed to geomagnetic field variations.

6. Conclusions

A general model has been developed for initial NRM acquisition near the sediment-water interface and inside the surface mixed layer. This model considers individual particles—defined as the smallest sediment units with elastic body behavior—under the influence of (1) magnetic torques, τ_m, which tend to align magnetic moments with the Earth's field, (2) holding torques, τ_h, which arise from interparticle interactions (e.g., hard contacts, Van der Waals, and electrostatic), and (3) random perturbing torques, τ_p, associated with Brownian motion, turbulence (in the water column), and bioturbation (in sediment). The sum of magnetic and holding torques is described by properly constructed random potentials with a given number of local minima. In the absence of perturbations (i.e., $\tau_p=0$), stable particle orientations coincide with these minima. Irreversible particle rotation is produced by perturbing torques upon overcoming the energy barriers between local minima of the random potential. A sequence of such irreversible events is equivalent to a rotational diffusion process with diffusion coefficient D_r. This process is formally described by a Smoluchowski-Debye equation (equation (6)), whose stationary solution is a Boltzmann distribution of magnetic moments (equation (7)). The Boltzmann distribution defines the remanent magnetization resulting from a dynamic equilibrium between the long-term action of aligning torques (τ_m) on the one hand, and the average effect of random torques (τ_p and τ_h) on the other hand (equation (18)). Dynamic equilibrium is reached within a typical time that is inversely proportional to D_r (equation (5)).

The magnitudes of D_r, τ_p, and τ_h evolve during different stages of NRM acquisition (Figure 1). Holding torques are completely absent inside the water column (i.e., $\tau_h=0$), and relatively weak perturbations allow the growth of loose particle aggregates (i.e., flocs). The concentration of flocs increases sharply across the sediment-water interface, where mechanical interactions, and thus τ_h, start to build up. The DRM acquired

in this region is still unstable, due to the small holding forces. DRM intensities are governed by a Langevin law (equation (12)), whereby relatively large acquisition efficiencies and nonlinear field dependencies are obtained if $\tau_p \leq \tau_m$. As flocs become buried inside the surface mixed layer, τ_h increases proportionally to the mechanical strength of sediment. Bioturbation produces irreversible magnetic moment reorientations in all cases where $\tau_p \geq \tau_h$, so that DRM is progressively replaced by a new, so-called mixing remanent magnetization (MRM). Because perturbing torques produced by bioturbation are presumably much stronger than those encountered in the water column, MRM intensity is expected to be smaller than DRM intensity (equation (18)).

The amounts of surviving DRM and acquired MRM at each depth below the sediment-water interface are controlled by a lock-in function (equation (29)), whose shape is mainly determined by the so-called rotation diffusivity parameter $\gamma = D_r L/\omega$, where L is the thickness of the surface mixed layer, and ω is the sedimentation rate. DRM is preserved as the only NRM contribution if $\gamma < 0.2$ (slow mixing regimes) and is completely replaced by a MRM for $\gamma > 10$ (fast mixing regimes). The strongest changes in NRM acquisition efficiency are thus expected for intermediate mixing regimes characterized by $0.2 < \gamma < 10$. Estimates of γ depend critically on D_r, for which direct measurements are not available. Lower D_r limits, obtained from minimum bioturbation rates expected from motile microorganisms, suggest that slow, fast, and intermediate mixing regimes exist for different sedimentary settings (Table 1).

The above mentioned DRM and MRM acquisition processes can introduce relative paleointensity artifacts in addition to those generated by normalization with laboratory magnetizations [*Roberts et al*., 2012]. Accordingly, we distinguish two main categories: (1) artifacts introduced by NRM acquisition efficiency variations in terms of remanence carrier alignment (e.g., DRM and MRM fractions) and (2) artifacts introduced by magnetic components with different intrinsic ratios between their NRM contributions and a normalizer magnetization (e.g., IRM and ARM). For example, intact magnetofossils have saturated magnetic moments that yield larger NRM/IRM and NRM/ARM values compared to other remanence carriers with the same degree of alignment. Variable combinations of the two artifact sources can generate contradictory or ambiguous results. For example, *Ouyang et al*. [2014] reported NRM/ARM ratios that are 2–4 times higher for biogenic magnetite with respect to a detrital component, while *Channell et al*. [2013] did not report significant differences between the two components.

Ambiguities associated with paleointensity artifacts are clearly illustrated with the example of the eastern equatorial Pacific sediment cores described by *Yamazaki et al*. [2013], where an inverse correlation has been observed between NRM acquisition efficiency (i.e., NRM/IRM) and a proxy for magnetizations due to magnetofossils (i.e., ARM/IRM). This correlation can be explained as an artifact of category 1 or 2, or both. In the first case, increased ARM/IRM values can be associated with faster bioturbation, assuming that magnetotactic bacteria represent a certain fraction of the benthic biomass. Faster bioturbation is characterized by higher D_r and L values and is driven by larger nutrient supplies. Nutrient supply is in turn supported by primary production and/or increased mineral fluxes [*Sarmiento and Gruber*, 2006], the latter being directly related to the sedimentation rate ω. The net effect of these changes on pelagic sediment mixing depends on the coupled parameters D_r, L, and ω: the combined increase of D_r and L likely exceeds corresponding variations of ω. In this case, γ is expected to covary with magnetofossil concentrations. The slow-to-intermediate mixing regime deducible from Table 1 for the locations analyzed by *Yamazaki et al*. [2013] would react to increased γ with a decrease of the overall NRM acquisition efficiency (i.e., NRM/IRM), due to DRM randomization (Figure 8). This mechanism can explain the inverse correlation between NRM/IRM and ARM/IRM observed by *Yamazaki et al*. [2013], with the lowest NRM/IRM values being typical of magnetofossil MRM acquisition, as well as the weak correlation with sedimentation rate. On the other hand, two magnetic components with the same NRM acquisition efficiency (e.g., in terms of NRM/IRM) but different ARM/IRM values (as is the case for detrital and magnetofossil components, see *Egli* [2004]) will generate an inverse correlation between NRM/IRM and ARM/IRM.

Our analytical models provide testable predictions about possible effects of sedimentary environments on NRM acquisition. Dedicated experiments are needed to obtain reliable estimates of bioturbation rates and mechanical sediment properties. A better knowledge of these parameters could lead to successful correction of variable NRM acquisition efficiencies in relative paleointensity records and to selection of the most reliable records on the basis of favorable sedimentary settings rather than limited variations of rock magnetic properties.

Acknowledgments
All results in this paper have been generated numerically using equations and methods explained in the text. X. Zhao was supported by the German Research Foundation (grant EG294/2-1) and Ludwig-Maximilians University. We are grateful to Andrew Roberts, Lisa Tauxe, an anonymous reviewer, and the Associated Editor, David Heslop, for constructive comments that helped to improve this paper.

References

Alexiewicz, A. (2000), Ensemble averages for Smoluchowski-Debye rotational diffusion in the presence of a two-angle-dependent reorienting force, *Chem. Phys. Lett.*, *320*, 582–586.
Anderson, R. F., R. F. Bopp, K. O. Buesseler, and P. E. Biscaye (1988), Mixing of particles and organic constituents from the continental shelf and slope off Cape Cod: SEEP-I results, *Cont. Shelf Res.*, *8*, 925–946.
Arason, P., and S. Levi (1990), Models of inclination shallowing during sediment compaction, *J. Geophys. Res.*, *95*, 4481–4499.
Barnes, H. A. (1997), Thioxotropy—A review, *J. Non Newtonian Fluid Mech.*, *70*, 1–33.
Bentley, S. J., A. Sheremet, and J. M. Jaeger (2006), Event sedimentation, bioturbation, and preserved sedimentary fabric: Field and model comparisons in three contrasting marine settings, *Cont. Shelf Res.*, *26*, 2108–2124.
Berg, H. C. (1983), *Random Walks in Biology*, Princeton Univ. Press, Princeton, N. J.
Berner, R. A. (1980), *Early Diagenesis: A Theoretical Approach*, Princeton Univ. Press, Princeton, N. J.
Bilardello, D., J. Jezek, and S. Gilder (2013), Numerical simulation of inclination shallowing by rolling and slipping of spherical particles, *Phys. Earth Planet. Inter.*, *214*, 1–13.
Bleil, U., and T. von Dobeneck (1999), Geomagnetic events and relative paleointensity records—Clues to high-resolution paleomagnetic chronostratigraphies of late Quaternary marine sediments?, in *Use of Proxies in Paleoceanography: Examples From the South Atlantic*, edited by G. Fischer and G. Wefer, pp. 635–654, Springer, Berlin Heidelberg.
Boudreau, B. P. (1986a), Mathematics of tracer mixing in sediments: I. Spatially-dependent, diffusive mixing, *Am. J. Sci.*, *286*, 161–198.
Boudreau, B. P. (1986b), Mathematics of tracer mixing in sediments: II. Nonlocal mixing and biological conveyor-belt phenomena, *Am. J. Sci.*, *286*, 199–238.
Boudreau, B. P. (1994), Is burial velocity a master parameter for bioturbation?, *Geochim. Cosmochim. Acta*, *58*, 1243–1249.
Boudreau, B. P. (1998), Mean mixed depth of sediments: The wherefore and the why, *Limnol. Oceanogr.*, *43*, 524–526.
Channell, J. E. T., and Y. Guyodo (2004), The Matuyama Chronozone at ODP Site 982 (Rockall Bank): Evidence for decimeter-scale magnetization lock-in depths, in Timescales of the Paleomagnetic Field, *Geophys. Monogr. Ser.*, vol. 145, edited by J. E. T. Channell et al., pp. 205–219, AGU, Washington, D. C.
Channell, J. E. T., D. A. Hodell, V. Margari, L. C. Skinner, P. C. Tzedakis, and M. S. Kesler (2013), Biogenic magnetite, detrital hematite, and relative paleointensity in Quaternary sediments from the Southwest Iberian Margin, *Earth Planet. Sci. Lett.*, *376*, 99–109.
Cole, J. J., M. L. Pace, N. F. Caraco, and G. S. Steinhart (1993), Bacterial biomass and cell size distributions in lakes: More and larger cells in anoxic waters, *Limnol. Oceanogr.*, *38*, 1627–1632.
Constable, C. G., and R. L. Parker (1998), Statistics of the geomagnetic secular variation for the past 5 m.y., *J. Geophys. Res.*, *93*, 11,569–11,581.
Dorgan, K. M., P. A. Jumars, B. D. Johnson, B. P. Boudreau and E. Landis (2005), Burrow extension by crack propagation, *Nature*, *433*, 475.
Egli, R. (2004), Characterization of individual rock magnetic components by analysis of remanence curves, 1. Unmixing natural sediments, *Stud. Geophys. Geod.*, *48*, 391–446.
Fenchel, T. (2001), Eppur si muove: Many water column bacteria are motile, *Aquat. Microbial Ecol.*, *24*, 197–201.
Fisher, R. (1953), Dispersion on a sphere, *Proc. R. Soc. London, Ser. A*, *217*, 295–305.
Frankel, R. B., and R. P. Blakemore (1980), Navigational compass in magnetic bacteria, *J. Magn. Magn. Mater.*, *15–18*, 1562–1564.
Galindo-González, C., et al. (2009), Magnetic and microscopic characterization of magnetite nanoparticles adhered to clay surfaces, *Am. Mineral.*, *94*, 1120–1129.
Geibert, W., M. M. Rutgers van der Loeff, R. Usbeck, R. Gersonde, G. Kuhn, and J. Seeberg-Elverfeldt (2005), Quantifying the opal belt in the Atlantic and southeast Pacific sector of the Southern Ocean by means of ^{230}Th normalization, *Global Biogeochem. Cycles*, *19*, GB4001, doi:10.1029/2005GB002465.
Griffiths, D. H., R. F. King, A. I. Rees, and A. E. Wright (1960), Remanent magnetism of some recent varved sediments, *Proc. R. Soc. London, Ser. A*, *256*, 359–383.
Hammond, D. E., J. McManus, W. M. Berelson, T. E. Kilgore, and R. H. Hope (1996), Early diagenesis of organic material in equatorial Pacific sediments: Stoichiometry and kinetics, *Deep Sea Res., Part II*, *43*, 1365–1412.
Hanzlik, M., M. Winklhofer, and N. Petersen (2002), Pulsed-field-remanence measurements on individual magnetotactic bacteria, *J. Magn. Magn. Mater.*, *248*, 258–267.
Heslop, D. (2007), Are hydrodynamic shape effects important when modelling the formation of depositional remanent magnetization?, *Geophys. J. Int.*, *165*, 775–785.
Heslop, D., A. P. Roberts, L. Chang, M. Davies, A. Abrajevitch, and P. De Dekker (2013), Quantifying magnetite magnetofossil contributions to sedimentary magnetizations, *Earth Planet. Sci. Lett.*, *382*, 58–65.
Jabbari-Farouji, S., G. H. Wegdam, and D. Bonn (2012), Aging of rotational diffusion in colloidal gels and glasses, *Phys. Rev. E*, *86*, 041401, 1–7.
Jezek, J., S. Gilder, and D. Bilardello (2012), Numerical simulation of inclination shallowing by rolling and slipping of spherical particles, *Comput. Geosci.*, *49*, 270–277.
Johnson, B. D., M. A. Barry, B. P. Boudreau, P. A. Dumas and K. M. Morgan (2012), In situ tensile fracture thoughness of surficial cohesive marine sediments, *Geo Mar. Lett.*, *32*, 39–48.
Kallmeyer, J., R. Pockalny, R. R. Adhikari, D. C. Smith, and S. D'Hondt (2012), Global distribution of microbial abundance and biomass in subseafloor sediment, *Proc. Natl. Acad. Sci. U. S. A.*, *109*, 16,213–16,216.
Katari, K., and L. Tauxe (2000), Effects of pH and salinity on the intensity of magnetization in redeposited sediments, *Earth Planet. Sci. Lett.*, *181*, 489–496.
Katari, K., L. Tauxe, and J. King (2000), A reassessment of post-depositional remanent magnetism: Preliminary experiments with natural sediments, *Earth Planet. Sci. Lett.*, *183*, 147–160.
Kent, D. V. (1973), Post-depositional remanent magnetization in deep-sea sediment, *Nature*, *246*, 32–34.
Kim, M., S. M. Anthony, S. C. Bae, and S. Granick (2011), Colloidal rotation near the colloidal glass transition, *J. Chem. Phys.*, *135*, 054905.
King, R. F. (1955), The remanent magnetism of artificially deposited sediments, *Geophys. J. Int.*, *7*, 115–134, doi:10.1111/j.1365-246X.1955.tb06558.x.
Koenderink, G. H., H. Zhang, D. G. A. L. Aarts, M. P. Lettinga, A. P. Philipse, and G. Nägele (2003), On the validity of Stokes-Einstein-Debye relations for rotational diffusion in colloidal suspensions, *Faraday Discuss.*, *123*, 335–354.
Larrasoaña, J. C., Q. Liu, P. Hu, A. P. Roberts, P. Mata, J. Civis, F. J. Sierro, and J. N. Pérez-Asensio (2014), Paleomagnetic and paleoenvironmental implications of magnetofossil occurrences in late Miocene marine sediments from the Guadalquivir Basin, SW Spain, *Frontiers Microbiol.*, *5*, 1–15, doi:10.3389/fmicb.2014.00071.

Locat, J., H. Lee, R. Kayen, M. C. Savoie, and E. Boulanger (2002), Shear strength development with burial in Eel river margin slope sediments, *Mar. Georesour. Ceochronol.*, *20*, 111–135.

Ludwig, P., R. Egli, S. Bishop, V. Chernenko, T. Frederichs, G. Rugel, and S. Merchel (2013), Characterization of primary and secondary magnetite in marine sediment by combining chemical and magnetic unmixing techniques, *Global Planet. Change*, *110*, 321–339, doi: 10.1016/j.gloplacha.2013.08.018.

Mao, X., R. Egli, N. Petersen, M. Hanzlik, and X. Zhao (2014a), Magnetotaxis and acquisition of detrital remanent magnetization by magnetotactic bacteria in natural sediment: First experimental results and theory, *Geochem. Geophys. Geosyst.*, *15*, 255–283, doi:10.1002/2013GC005034.

Mao, X., R. Egli, N. Petersen, M. Hanzlik, and X. Liu (2014b), Magneto-chemotaxis in sediment: First insights, *PLoS ONE*, *9*, e102810, 1–14, doi:10.1371/journal.pone.0102810.

Martinez, V. A., R. Besseling, O. A. Croze, J. Tailleur, M. Reufer, J. Schwarz-Linek, L. G. Wilson, M. A. Bees, and W. C. K. Poon (2012), Differential dynamic microscopy: A high-throughput method for characterizing the motility of microorganisms, *J. Biophys.*, *103*, 1637–1647.

McNeill, D. F., and J. L. Kirschvink (1993), Early dolomitization of platform carbonates and the preservation of magnetic polarity, *J. Geophys. Res.*, *98*, 7977–7986.

Meadows, P. S., and J. Tait (1989), Modification of sediment permeability and shear strength by two burrowing invertebrates, *Mar. Biol.*, *101*, 75–82.

Meysman, F. J. R., B. P. Boudreau and J. J. Middelburg (2003), Relations between local, nonlocal, discrete, and continuous models of bioturbation, *J. Mar. Res.*, *61*, 391–410.

Mitchell, J. G., and K. Kogure (2006), Bacterial motility: Links to the environment and driving force for microbial physics, *FEMS Microbiol. Ecol.*, *55*, 3–16.

Mitra, R., and L. Tauxe (2009), Full vector model for magnetization in sediments, *Earth Planet. Sci. Lett.*, *286*, 535–545.

Ouyang, T., D. Heslop, A. P. Roberts, C. Tian, Z. Zhu, Y. Qiu and X. Peng (2014), Variable remanence acquisition efficiency in sediments containing biogenic and detrital magnetites: Implications for relative paleointensity signal recording, *Geochem. Geophys. Geosyst.*, *15*, 2780–2796, doi:10.1002/2014GC005301.

Pemberton, G. S., M. J. Risk, and D. E. Buckley (1976), Supershrimp: Deep bioturbation in the Strait of Canso, Nova Scotia, *Science*, *192*, 790–791.

Perrin, F. (1934), The Brownian movement of an ellipsoid (I)—The dielectric dispersion of ellipsoidal molecules, *J. Phys. Radium*, *5*, 497–511.

Perrin, F. (1936), The Brownian movement of an ellipsoid (II) - Free rotation and depolarization of fluorescences. Translation and diffusion of ellipsoidal molecules, *J. Phys. Radium*, *7*, 1–11.

Pisias, N. G., L. A. Mayer, and A. C. Mix (1995), Paleoceanography of the eastern equatorial Pacific during the Neogene: Synthesis of Leg 138 drilling results, in *Proceedings of the Ocean Drilling Program, Scientific Results*, vol. 138, edited by N. G. Pisias *et al*., pp. 5–21, Ocean Drill. Program, College Station, Tex.

Rabouille, C., and J. F. Gaillard (1991), A coupled model representing the deep-sea organic carbon mineralization and oxygen consumption in surficial sediments, *J. Geophys. Res.*, *96*, 2761–2776.

Reed, D. C., K. Huang, B. P. Boudreau and F. J. R. Meysman (2006), Steady-state tracer dynamics in a lattice-automaton model of bioturbation, *Geophys. Cosmochim. Acta*, *70*, 5855–5867.

Roberts, A. P., and M. Winklhofer (2004), Why are geomagnetic excursions not always recorded in sediments? Constraints from post-depositional remanent magnetization lock-in modelling, *Earth Planet. Sci. Lett.*, *227*, 345–359.

Roberts, A. P., L. Chang, D. Heslop, F. Florindo and J. C. Larrasoaña (2012), Searching for single domain magnetite in the "pseudo-single-domain" sedimentary haystack: Implications of biogenic magnetite preservation for sediment magnetism and relative paleointensity determinations, *J. Geophys. Res.*, *117*, B08104, doi:10.1029/2012JB009412.

Roberts, A. P., L. Tauxe and D. Heslop (2013), Magnetic paleointensity stratigraphy and high-resolution Quaternary geochronology: Successes and future challenges, *Quat. Sci. Rev.*, *61*, 1–16.

Sagnotti, L., F. Budillon, J. Dinarès-Turell, M. Iorio, and P. Macrí (2005), Evidence for a variable paleomagnetic lock-in depth in the Holocene sequence from the Salerno Gulf (Italy): implications for "high-resolution" paleomagnetic dating, *Geochem. Geophys. Geosyst.*, *6*, Q11013, doi:10.1029/2005GC001043.

Sarmiento, J. L., and N. Gruber (2006), *Ocean Biogeochemical Dynamics*, Princeton Univ. Press, Princeton, N. J.

Šestanović, S., M. Šolić, N. Krstulović, and D. Bogner (2005), Volume, abundance, and biomass of sediment bacteria in the eastern mid Adriatic Sea, *Acta Adriatica*, *46*, 177–191.

Shcherbakov, V. P., and V. V. Shcherbakova (1987), On the physics of acquisition of post-depositional remanent magnetization, *Phys. Earth Planet. Inter.*, *46*, 64–70.

Shcherbakov, V. P., and N. Sycheva (2010), On the mechanism of formation of depositional remanent magnetization, *Geophys. Geochem. Geosyst.*, *11*, Q02Z13, doi:10.1029/2009GC002830.

Shull, D. H. (2001), Transition-matrix model of bioturbation and radionuclide diagenesis, *Limnol. Oceanogr.*, *46*, 905–916.

Smith, C. R., and C. Rabouille (2002), What controls the mixed-layer depth in deep-sea sediments? The importance of POC flux, *Limnol. Oceanogr.*, *47*, 418–426.

Solan, M., B. D. Wigham, I. R. Hudson, R. Kennedy, C. H. Coulon, K. Norling, H. C. Nilsson, and R. Rosenberg (2004), In situ quantification of bioturbation using time-lapse fluorescent sediment profile imaging (f-SPI), luminophore tracers and model simulation, *Mar. Ecol. Prog. Ser.*, *271*, 1–12.

Suganuma, Y., J. Okuno, D. Heslop, A. P. Roberts, T. Yamazaki and Y. Yokoyama (2011), Post-depositional remanent magnetization lock-in for marine sediments deduced from ^{10}Be and paleomagnetic records through the Matuyama-Brunhes boundary, *Earth Planet. Sci. Lett.*, *311*, 39–52.

Sverdrup, H. U., M. W. Johnson, and R. H. Fleming (1942), *The Oceans, Their Physics, Chemistry, and General Biology*, Prentice-Hall, N. Y.

Tarduno, J. A., and S. L. Wilkison (1996), Non steady state magnetic mineral reduction, chemical lock-in, and delayed remanence acquisition in pelagic sediments, *Earth Planet. Sci. Lett.*, *144*, 315–326.

Tarduno, J. A., W. Tian, and S. Wilkison (1998), Biogeochemical remanent magnetization in pelagic sediments of the western equatorial Pacific Ocean, *Geophys. Res. Lett.*, *25*, 3987–3990.

Tauxe, L., and D. V. Kent (2004), A simplified statistical model for the geomagnetic field and the detection of shallow bias in paleomagnetic inclinations: Was the ancient magnetic field dipolar?, in *Timescales of the Paleomagnetic Field, Geophys. Monogr. Ser.*, vol. 145, AGU, Washington, D. C., doi:10.1029/145GM08.

Tauxe, L., J. L. Steindorf, and A. Harris (2006), Depositional remanent magnetization: Toward and improved theoretical and experimental foundation, *Earth Planet. Sci. Lett.*, *244*, 515–529.

Teal, L. R., M. T. Bulling, E. R. Parker, and M. Solan (2008), Global patterns of bioturbation intensity and mixed depth of marine soft sediments, *Aquat. Biol.*, *2*, 207–218.

Torquato, S. (1995), Nearest-neighbor statistics for packings of hard spheres and disks, *Phys. Rev. E*, *51*, 3170–3182.

Trauth, M. H., M. Sarnthein, and M. Arnold (1997), Bioturbational mixing depth and carbon flux at the seafloor, *Paleoceanography*, *12*, 517–526.

Tucker, P. (1980), A grain mobility model of post-depositional realignment, *Geophys. J. R. Astron. Soc.*, *63*, 149–163.

Van Vreumingen, M. (1993), The magnetization intensity of some artificial suspensions while flocculating in a magnetic field, *Geophys. J. Int.*, *114*, 601–606.

Weitz, D. A. (2011), Colloidal glasses, in *Glasses and Grains: Poincaré Seminar 2009*, edited by B. Duplantier, T.C. Halsey, and V. Rivasseau, pp. 25–39, Springer, Basel, Switzerland.

Wilson, L. G., V. A. Martinez, J. Schwarz-Linek, J. Tailleur, P. N. Pusey, and W. C. K. Poon (2011), Differential dynamic microscopy of bacterial motility, *Phys. Rev. Lett.*, *106*, 018101, 1–4.

Winch, D. E., D. J. Ivers, J. P. R. Turner, and R. J. Stening (2005), Geomagnetism and Schmidt quasi-normalization, *Geophys. J. Int.*, *160*, 487–504.

Won, J. Y. (2013), Anisotropic strength ration and plasticity index of natural clays, in *Proceedings of the 18th International Conference on Soil Mechanics and Geotechnical Engineering*, pp. 445–448, International Society for Soil Mechanics and Geotechnical Engineering, Paris.

Yamazaki, T., Y. Yamamoto, G. Acton, E. P. Guidry, and C. Richter (2013), Rock-magnetic artifacts on long-term relative paleointensity variations in sediments, *Geochem. Geophys. Geosyst.*, *14*, 29–43, doi:10.1019/2012GC004546.